

PSYM-WIDE: A SURVEY FOR LARGE-SEPARATION PLANETARY-MASS COMPANIONS TO LATE SPECTRAL TYPE MEMBERS OF YOUNG MOVING GROUPS

MARIE-EVE NAUD^{1*}, ÉTIENNE ARTIGAU¹, RENÉ DOYON¹, LISON MALO^{2,1}, JONATHAN GAGNÉ^{3,4}, DAVID LAFRENIÈRE¹, CHRISTIAN WOLF⁵ AND EUGENE A. MAGNIER⁶

¹ Institut de recherche sur les exoplanètes, Département de physique, Université de Montréal, Montréal, QC H3C 3J7, Canada.

² Canada-France-Hawaii Telescope (CFHT) Corporation, 65-1238 Mamalahoa Highway, Kamuela, HI 96743, USA.

³ Department of Terrestrial Magnetism, Carnegie Institution for Science, 5241 Broad Branch Road NW, Washington, DC 20015, USA.

⁴ NASA Sagan Fellow

⁵ Research School of Astronomy and Astrophysics, Australian National University, Canberra, ACT 2611, Australia

⁶ Institute for Astronomy, University of Hawaii, 2680 Woodlawn Drive, Honolulu, HI 96822, USA.

ABSTRACT

We present the results of a direct-imaging survey for very large separation (>100 au), companions around 95 nearby young K5–L5 stars and brown dwarfs. They are high-likelihood candidates or confirmed members of the young ($\lesssim 150$ Myr) β Pictoris and AB Doradus moving groups (ABDMG) and the TW Hya, Tucana-Horologium, Columba, Carina, and Argus associations. Images in i' and z' filters were obtained with the Gemini Multi-Object Spectrograph (GMOS) on Gemini South to search for companions down to an apparent magnitude of $z' \sim 22$ –24 at separations $\gtrsim 20''$ from the targets and in the remainder of the wide 5.5×5.5 GMOS field of view. This allowed us to probe the most distant region where planetary-mass companions could be gravitationally bound to the targets. This region was left largely unstudied by past high-contrast imaging surveys, which probed much closer-in separations. This survey led to the discovery of a planetary-mass (9 – $13 M_{\text{Jup}}$) companion at 2000 au from the M3V star GU Psc, a highly probable member of ABDMG. No other substellar companions were identified. These results allowed us to constrain the frequency of distant planetary-mass companions (5 – $13 M_{\text{Jup}}$) to $0.84^{+6.73}_{-0.66}\%$ (95% confidence) at semimajor axes between 500 and 5000 au around young K5–L5 stars and brown dwarfs. This is consistent with other studies suggesting that gravitationally bound planetary-mass companions at wide separations from low-mass stars are relatively rare.

Keywords: planets and satellites: detection – planets and satellites: gaseous planets – stars: individual (GU Psc) – stars: low-mass

1. INTRODUCTION

Twenty years after the first detection of an exoplanet around a main-sequence star (Mayor & Queloz 1995), the increasing number of known exoplanets provides a clearer overall picture of the content and architecture of exoplanetary systems. However, the outer realms of planetary systems, inaccessible to the radial velocity and transit methods, are still largely unexplored. Direct imaging is the prime method for exploring separations larger than a few tens of astronomical units. This method has seen tremendous improvements since the first major discoveries, including the first image of a planetary-mass companion around the brown dwarf 2MASS J12073346-3932539 b (2M 1207 b here-

after; Gizis 2002; Chauvin et al. 2004; Ducourant et al. 2008), the first image of a planet around a sun-like star, 1RXS J1609-2105 b (Lafrenière et al. 2008, 2010) and the first exoplanetary system, around HR 8799 (Marois et al. 2008, 2010). Dedicated second-generation, high-contrast imagers like SPHERE (Beuzit et al. 2008) and GPI (Macintosh et al. 2014) are now reaching contrasts allowing the detection of giant planets from ~ 5 to ~ 100 au (Macintosh et al. 2015; Wagner et al. 2016).

While similar to their closer-in exoplanet counterparts in many ways, distant, directly imaged companions also share similarities with low-mass brown dwarf companions and isolated planetary-mass objects (e.g., Faherty et al. 2016). The directly imaged exoplanets found to date provide essential constraints on the dynamics of planetary systems and on substellar formation models and come with their own open questions. Most of them

*Corresponding author: naud@astro.umontreal.ca

are not readily explained by standard planetary formation scenarios. They could be planets formed in a disk that were later scattered outward or planetary-mass objects that formed like brown dwarfs and stars, through the fragmentation of a collapsing prestellar core.

Young stars are prime targets for direct imaging surveys, as young companions are brighter than their older counterparts, since they are still contracting and cooling down. Recently, significant progress has been made to identify young stars of the local neighborhood that are members of Young Moving Groups (YMGs). Stars in these sparse ensembles were formed together and therefore share similar positions and space motions in the Galaxy (Zuckerman & Song 2004). Their members provide an important advantage for direct imaging surveys, because evolutionary models allow us to translate their well-constrained age to relatively precise mass constraints for planetary-mass companions. Most low-mass late spectral type members of these associations remained undetected until a few years ago because the observations used to determine proper motions, radial velocities, and distances were mostly available in the optical. Malo et al. (2013; M13 hereafter), Malo et al. (2014b; M14 hereafter), and Gagné et al. (2014; G14 hereafter) identified a large number of low-mass stars, brown dwarfs, and isolated planetary-mass objects with high membership probabilities in seven young and nearby YMGs (the β Pictoris moving group, β PMG; the TW Hya association, TWA; the Tucana-Horologium association, THA; the Columba association, COL; the Carina association, CAR; the Argus association, ARG; and the AB Doradus moving group, ABDMG), using a novel Bayesian analysis and dedicated observation programs.

Some of the first direct imaging surveys concentrated on massive stars, where theory predicts more giant exoplanets and where some of the first detections of planets through direct imaging were made (notably, HR 8799, an A5V star; Marois et al. 2008, 2010). First-generation surveys, like the Gemini Deep Planet Survey (GDPS; Lafrenière et al. 2007) and the NaCo Deep imaging survey of young, nearby austral stars (Chauvin et al. 2010) did include several M stars. Interestingly, the latter led to the discovery of the planetary-mass companion around the M8 brown dwarf 2M1207. Surveys dedicated to low-mass stars were undertaken in recent years. The PALMS survey (Planets Around Low-Mass Stars; Bowler et al. 2015) did not detect any 1–13 M_{Jup} companions between 10–100 au around their sample of 122 K5–M4 single dwarfs. This allowed determination of an upper limit (95% confidence level) of 10.3% (16%) for these objects, assuming a hot (cold) start evolutionary model. Lammier et al. (2016) presents the results of another M-star survey, based on VLT observations. Their sample of 58 M stars includes most of the 16 stars from

the Delorme et al. (2012) survey, a pioneer study dedicated to low-mass stars. A frequency of $2.3^{+2.9}_{-0.7}\%$ is determined for 2–14 M_{Jup} companions at separations of 8–400 au. The meta-analysis presented by Bowler (2016), which summarizes the results of nine surveys (including PALMS, GDPS, and the Gemini NICI Planet-Finding Campaign; Biller et al. 2013), includes 118 M stars and finds an upper limit of 3.9% (5.4%; 7.3%) for the occurrence of 5–13 M_{Jup} at 30–300 au (10–1000 au; 100–1000 au) around them. The results of the IDPS (International Deep Planet Search) survey (292 stars) were combined with those of GDPS and of the NaCo-LP survey (Chauvin et al. 2015) in Galicher et al. (2016). They find a planetary-mass (0.3–14 M_{Jup}) companion fraction between 20–300 au of $0.90^{+4.05}_{-0.65}\%$ for their “low mass” ($<1.1 M_{\odot}$) sample, which includes G, K, and M stars.

In 2010, the survey PSYM – Planet Search around Young-associations M dwarfs – was started to detect planetary-mass companions around young K5–L5 stars and brown dwarfs newly identified in M13, M14, and G14. This paper presents the results of the PSYM-WIDE survey of 95 stars with the Gemini Multi-Object Spectrograph (GMOS; Hook et al. 2004) at Gemini South. PSYM-WIDE was designed specifically to detect planetary-mass companions at large (500–5000 au) separations. A new planetary-mass companion, GU Psc b, was identified as part of this survey and was presented by Naud et al. (2014). The sample and selection criteria are described in §2, and the observations are presented in §3, and followed by the results in §4. A discussion that puts the results derived in perspective is presented in §5. The paper concludes with a discussion on the plausible origin of these wide companions and ongoing efforts to find them.

2. THE STELLAR SAMPLE

2.1. Target Selection

The sample of stars surveyed in this work has been drawn primarily from high-probability YMG members identified by the Bayesian analysis presented in M13, M14, and G14. The BANYAN (M13, M14) and BANYAN II (G14) tools both use sky position, proper motion, and color-magnitude diagrams to assess the probability that a star is a member of β PMG, ABDMG, TWA, THA, COL, CAR, or ARG. The Bayesian analysis provides an estimation of the radial velocity and distance (statistical distance; d_s) of a star assuming membership to a given association. The statistical distance and predicted radial velocities have been demonstrated to have a typical accuracy of ~ 10 –20% compared to direct measurements when membership is confirmed (see M13). When a star has a high membership probability, this method therefore provides good estimates of those

values. Measuring the radial velocity or parallax together with other signs of youth is needed to unambiguously establish the membership of a candidate member.

In M13, the I_C and J photometry was used with the BANYAN tool to identify 214 new, highly probable low-mass members (spectral types K5–M5) among an initial sample of several hundreds of stars displaying youth indicators such as H_α or X-ray emission from Riaz et al. (2006). In M14, new radial velocity measurements were included in the analysis to further confirm the membership of 130 candidates from M13 and 57 other stars from the literature. The BANYAN II tool presented in G14 adapted the M13 analysis to identify lower-mass stars and brown dwarf (later than M7) members of the YMG, using 2MASS and *WISE* photometry. Their initial candidate sample is composed of 158 stars that display spectroscopic signs of youth or have unusually red colors for their spectral type at near-infrared wavelengths. Among these, 25 new high-probability candidates were identified, and the membership of 10 candidates was confirmed. The same tool was used in an all-sky survey built from a cross-match of the 2MASS and AllWISE to identify a total of 228 new M4–L6 candidate members of YMGs (Gagné et al. 2015b,c).

Among the M13/M14/G14 published or preliminary samples, those with declinations lower than $+20^\circ$ were first selected, as observations were to be made at Gemini South in Chile. Stars with the highest membership probabilities were prioritized. Stars in the youngest associations were preferred, as younger companions at a given mass are brighter than their older counterparts and thus easier to detect. Stars with the nearest statistical distances (or parallaxes when available) were also prioritized, in order to probe a region as close as possible to the stars. Objects located at distances beyond 80 pc were rejected. Binary stars were not excluded a priori from the selection. Twenty stars in the sample are known as double or triple systems. These are identified in the spectral type column of Table 1 with the mention “sb1”, “sb2” or “sb3”, or with the “+” sign, which indicates that there is a stellar companion (the spectral type of this companion is sometimes not known). Recent discoveries have demonstrated that the presence of a similar-mass or lower-mass companion does not preclude the detection of additional companions around a star; Ross 458(AB)c represents such a low-mass companion on a very wide orbit around a much tighter M-dwarf binary (Goldman et al. 2010). A total of 69 stars were taken from the M13/M14 sample, and 12 from G14.

Seven bona fide members previously known in the literature and used in M13 or G14 to determine the kinematic and photometric properties of the YMGs were also added to the sample. A few young stars that do not appear in M13, M14, or G14 but that were also identified

as young in the literature (three from Shkolnik et al. 2011, 2012, three from Rodriguez et al. 2011, and one from Kiss et al. 2011) were also included.

The properties of the final sample of 95 stars are listed in Table 1 and presented in Figures 1 and 2. They have late spectral types ranging from K5 to L5, with a median type of M3. The least massive of the stars in the sample are close to the deuterium-burning limit mass. For example, Faherty et al. (2016) estimated the mass of the L3 2MASS J21265040-8140293 to be $24.21 \pm 14.3 M_{Jup}$, and that of the L1 2MASS J00040288-6410358 to be $16.11 \pm 2.9 M_{Jup}$. No selection was made based on the galactic latitude; seven targets have galactic latitude $|b| < 15^\circ$, and are thus located in relatively crowded fields. This slightly complicates the confirmation procedure and reduces the likelihood of planet detection (see Section 4.2). It is important to note that the sample of young nearby stars from which we draw our sample is still under construction and suffers many biases (Riaz et al. 2006, for example, only selected the sources that are bright in X-ray). Therefore, it is not expected that it follows closely a field initial mass function.

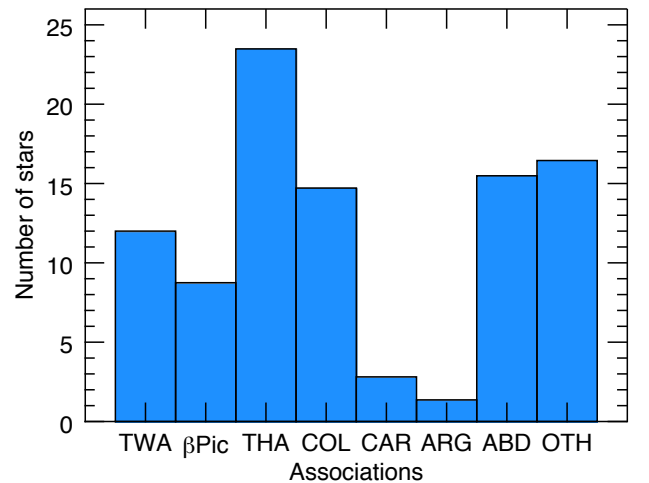


Figure 1. Distribution of the target stars most probable associations of the target stars.

2.2. Age and Distance estimates

A distance estimate for the target star is needed to convert angular separation to physical separation and apparent magnitude limits to absolute magnitude limits. An estimate of the age is also necessary to convert absolute magnitude to mass, using evolutionary models. Assigning membership to a young association is one of the few ways that are available to constrain the age of low-mass stars and obtain an approximation of their distance, as seen in Section 2.1. All targets selected for the PSYM-WIDE survey were analyzed with the most

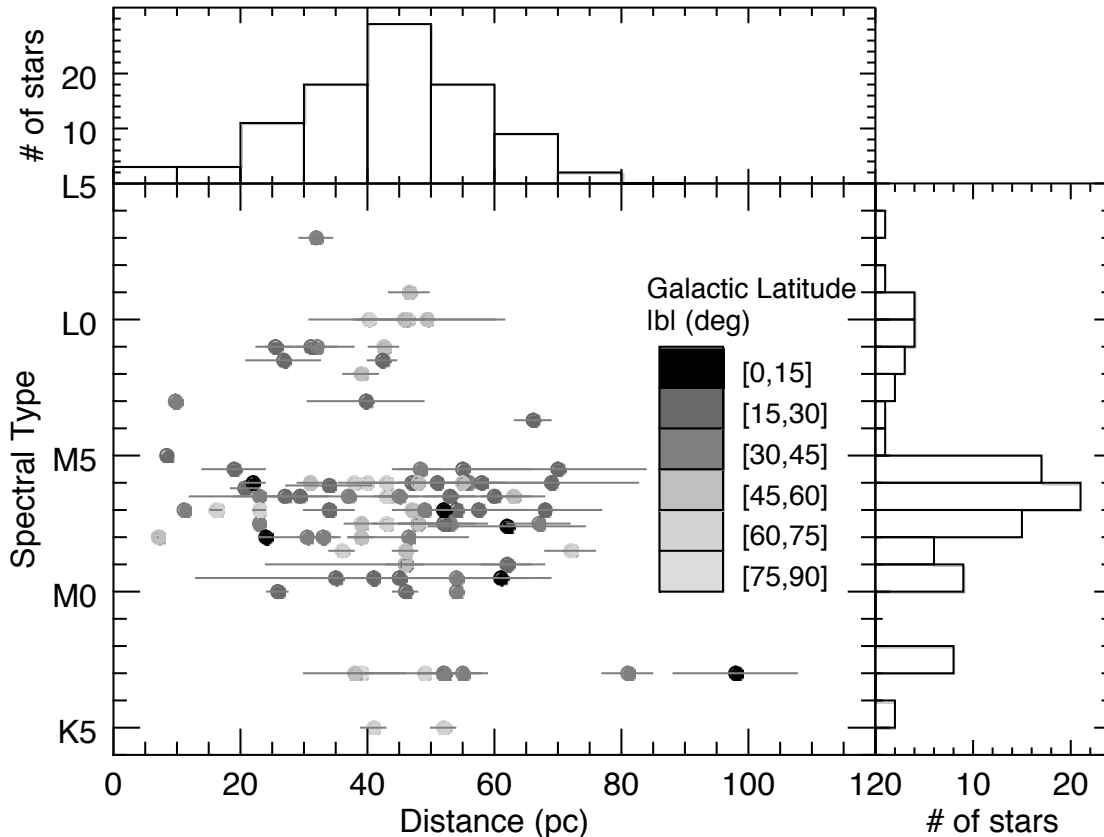


Figure 2. Distribution of spectral types vs. distribution of distances. The histograms of these values are also shown. The galactic latitude $|b|$ is color coded: the greater the distance from the galactic plane, the lighter the points are.

recent version of BANYAN (spectral type earlier than M7) or BANYAN II (spectral type later than M7) to calculate their membership probability to several YGMs, informed by the most recent measurements of proper motion, parallax, and radial velocity. The membership of all stars is listed in Table 2.

The status “bona fide” (BF) was assigned to stars with all kinematic measurements, a trigonometric parallax, and youth indicators that have a Bayesian probability above a selected high threshold ($>90\%$ for stars analyzed with BANYAN and $>99\%$ for those analyzed with BANYAN II) that minimizes the chance of a false positive in the sample. Objects that are missing one kinematic measurement and have a Bayesian probability above the threshold are referred to as “high-likelihood candidates” (HLC). Those that have no radial velocity or parallax measurements with a Bayesian probability above the threshold are referred to as “candidates” (C). The large majority of the stars in the sample belong to one of these categories (7 BF, 58 HLC, and 2 C).

Ten stars have an ambiguous membership status (AY for “ambiguous membership, young”), because their membership probability is high in two or more of the

seven associations. Seventeen stars were assigned the status “young other” (YO). Such cases correspond to stars for which the BANYAN membership probability assigned is low but nonnegligible for at least one moving group, members of YMGs that are not known or not included in BANYAN, or simply relatively young stars that do not belong to a group. In one case, a star initially thought young was found to display no youth indicator. It has the status NYI (“no youth indicator”) in Table 2.

The histogram of Figure 1 shows the most probable association for all stars. Candidate members of TWA, β PMG, THA, and COL are the most numerous as they are the youngest associations and were thus favored in the sample construction. Several stars are also candidate members of ABDMG.

2.2.1. Age

For BF, HLC, C, and AY stars, the total age range of all the plausible association(s) is conservatively assigned to the star. The association age ranges determined in the recent analysis of Bell et al. (2015) are used here: β PMG: 24 ± 3 Myr; ABDMG: 149^{+51}_{-19} Myr; TWA: 10 ± 3 Myr; THA: 45 ± 4 Myr; COL: 42^{+5}_{-4} Myr;

CAR: 45_{-7}^{+11} Myr. For ARG, [Bell et al. \(2015\)](#) did not assign a final age, arguing that the list of members appears to be contaminated. According to their analysis, it is unclear that the members represent a single coeval population. Assessing whether this association is indeed a unique ensemble of coeval objects is beyond the scope of this paper, so the age range determined by [Makarov & Urban \(2000\)](#) (30–50 Myr) is used for ARG objects.

For YO stars, other age indicators were used to constrain the age of the star. Several low-mass stars from the [Riaz et al. \(2006\)](#) sample and analyzed by M13 for moving group membership have H_α emission measurements. Since H_α in emission remains for ~ 1 Gyr for early M dwarfs ([West et al. 2008](#)), this sets an upper age limit for these stars. The presence of lithium was also used to constrain the age of some stars. For some stars analyzed by BANYAN II (M7 or later types), the gravity classes of [Allers & Liu \(2013\)](#) were used. [Allers & Liu \(2013\)](#) have constructed a gravity classification scheme based on several spectral indices in the near-infrared that allows us to classify low-mass stars and brown dwarfs in one of three categories: field gravity (FLD-G), intermediate gravity (INT-G), and very low gravity (VL-G). The INT-G and VL-G gravity classes were built to correspond, respectively, to the β and γ visual classifications introduced by [Cruz et al. \(2009\)](#) and used in the spectral types listed in Table 1. The three classes respectively correspond to objects of decreasing surface gravities and thus likely decreasing ages. Using a sample of age-calibrated objects, they determined that the VL-G class corresponds to an age range of ~ 10 –30 Myr, and that the INT-G class corresponds to an age range of ~ 50 –200 Myr. They note that there are exceptions, but there is an observed trend where the fraction of VL-G objects with respect to INT-G or FLD-G objects is higher in younger moving groups ([Allers & Liu 2013](#); [Faherty et al. 2016](#)). When no other age constraints were available, spectral indices were used to assess if they belong to one of the two low-gravity classes. If it was the case, the stars were assigned 200 Myr as an upper bound; if not, they were assigned 200 Myr as a lower bound. When a lower or upper bound was not available for age, the values 5 Myr and 10,000 Myr were respectively conservatively assigned, assuming the stars are not in star-forming regions and do not belong to the thick disk or halo. Table 2 summarizes the adopted age range for all survey targets. The midrange age was computed for each star. The median of the midrange ages is ~ 45 Myr.

2.2.2. Distance

Trigonometric distances are used when available. This is the case for all BF stars, by definition. For HLC stars that do not have a trigonometric distance measurement,

the statistical distance in the most probable association is used. For AY stars, the total range of statistical distances in the associations that have high membership probabilities is assigned. For YO stars that do not benefit from a parallax measurement, the spectrophotometric distance (d_{sp}) was estimated from the method of [Gagné et al. \(2015a\)](#). Spectral types listed in Table 1 were used in combination with the spectral-type absolute-magnitude sequences of ~ 5 –200 Myr objects in a specific near-infrared (NIR) band to obtain a distance estimate and measurement error for a given object. These measurements were performed on the 2MASS J , H and K_S bands and the AllWISE $W1$ and $W2$ bands and were each represented by a Gaussian probability density function (PDF) with the appropriate central position and characteristic width. The five PDFs were then multiplied together to obtain a final measurement PDF; the maximum position of this PDF corresponds to the most probable distance, and the 68% range corresponds to measurement uncertainties. This method does not account for correlations between the different NIR magnitudes of young objects and may thus slightly underestimate the measurement errors (see [Gagné et al. 2015a](#) for more detail). Table 2 and Figure 2 summarize the adopted distance ranges. The median distance of the sample is ~ 45 pc.

3. OBSERVATION AND DATA REDUCTION

3.1. Observing Strategy

In this survey, planetary-mass companions are identified via their distinctively high $i' - z'$ color. This strategy was previously used to identify a number of T dwarfs in the Canada-France Brown Dwarf Survey ([Delorme et al. 2008](#); [Albert et al. 2011](#)). This is because low-mass objects give off most of their flux in the infrared. Figure 3 shows that the rise of the flux around 780 nm in the SED of brown dwarfs is steeper for late spectral types, which results in an $i' - z'$ increasing from $i' - z' \sim 2$ for types earlier than L4 to $i' - z' \sim 3$ for L8 and $i' - z' \sim 4$ for T3 ([Zhang et al. 2009](#)).

Figure 4 shows the apparent z' magnitude versus $i' - z'$ for all objects identified in the field of one of the targets, 2MASS J06131330-2742054. Typical fields L0–T4 are also shown, with the apparent magnitudes they would have at the mean distance of the target, 29 pc ([West et al. 2005](#); [Zhang et al. 2009](#)). For each spectral type, the dot corresponds to the value of a field object. Younger objects are expected to have inflated radii ([Chabrier et al. 2000](#)) and would thus appear slightly brighter and thus higher on the figure. The vast majority of objects in a given field are much bluer (to the left) than the $i' - z' = 1.7$ threshold adopted. Very few false positives are thus expected. Besides young low-

Table 1. Target Sample Properties

2MASS Designation	Coordinates		Proper Motion		Sp. Type ^{a, b} (Opt.)	Magnitudes			Trigonometric distance ^b (pc)	Radial Velocity ^b (km s ⁻¹)		
	α (J2000.0)	δ (J2000.0)	$\mu_\alpha \cos \delta$ (mas yr ⁻¹)	μ_δ (mas yr ⁻¹)		Ref. ^b	H	K_S			J	W1
J00040288-6410358	1.0120	-64.1766	64.0±12.0	-47.0±12.0	F16		14.83	14.01	13.41	12.96	5.3 ± 3.4 ^l	
J00172353-6645124	4.3481	-66.7535	102.9±1.0	-15.0±1.0	Z12		7.93	7.70	7.59	7.50	10.7 ± 0.2	
J00325584-4405058	8.2327	-44.0850	128.3±3.4	-93.6±3.0	F16		14.78	13.86	13.27	12.84	12.9 ± 1.9 ^k	
J00374306-5846229	9.4294	-58.7730	57.0±10.0	17.0±5.0	F16		15.37	14.26	13.59	13.15	6.6 ± 0.1 ^k	
J01071194-1935359	16.7998	-19.5933	64.4±1.6	-39.5±1.2	Z12	M0.5+M2.5 ^c	8.15	7.47	7.25	7.09	11.5 ± 1.4 ^P	
J01123504+1703557	18.1460	17.0655	92.0±1.0	-98.4±1.0	Z05	M3	10.21	9.60	9.35	9.26	9.13	-1.5 ± 0.5
J01132958-0738088	18.3733	-7.6358	70.5±1.1	-66.1±1.0	Z12	K7+M5.5 ⁿ	9.36	8.71	8.53	8.43	8.41	41.3 ± 4.1
J01220441-3337036	20.5184	-33.6177	105.3±1.2	-58.3±1.0	Z12	K7	9.92	8.31	7.64	7.45	7.27	4.7 ± 0.4
J01351393-0712517	23.8080	-7.2144	106.5±5.1	-60.7±5.1	Ro10	M4(sb2) ^{v, s}	8.96	8.39	8.08	7.97	7.80	6.8 ± 0.8
J01415823-4633574	25.4926	-46.5660	105.0±10.0	-49±10	F16	L0 γ^g	14.83	13.88	13.10	12.58	12.19	6.4 ± 1.6 ^k
J01484087-4830519	27.1703	-48.5144	110.3±1.1	-51.0±1.1	Z12	M1.5	9.19	8.55	8.36	8.26	8.19	21.5 ± 0.2
J01521830-5950168	28.0763	-59.8380	109.2±1.8	-25.7±1.8	Z12	M2-3 ^P	8.94	8.33	8.14	7.96	7.88	8.1 ± 1.8
J02045317-5346162	31.2216	-53.7712	95.1±2.9	-33.6±3.1	Z12	K5	10.44	9.81	9.56	9.41	9.22	10.9 ± 0.3
J02070176-4406380	31.7573	-44.1106	94.9±1.3	-30.6±1.3	Z12	M3.5(sb1) ^{v, s}	9.27	8.69	8.40	8.25	8.09	10.1 ± 0.3
J02155892-0929121	33.9955	-9.4867	96.6±1.9	-46.5±2.6	Z12	M2.5(sb3) ^{v, s}	8.43	7.80	7.55	7.31	7.26	2.5 ± 0.3
J02215494-5412054	35.4790	-54.2015	136.0±10.0	-10.0±17.0	F16	M8 β^u	13.90	13.22	12.66	12.34	11.97	10.2 ± 0.1 ^k
J02224418-6022476	35.6841	-60.3799	137.4±1.7	-13.8±1.7	Z12	M4	8.99	8.39	8.10	7.95	7.80	13.1 ± 0.9
J02251947-5837295	36.3311	-58.6249	102.2±5.2	-25.0±7.3	2MAW	M9 β^k	13.74	13.06	12.56	12.26	11.96	
J02303239-4342232	37.6350	-43.7065	80.3±0.9	-13.3±0.9	Z12	K5Ve ^{eee}	8.02	7.43	7.23	7.12	7.22	16.0 ± 1.3
J02340093-6442068	38.5039	-64.7019	88.0±12.0	-15.0±12.0	F16	L0 γ^o	15.32	14.44	13.85	13.27	12.93	11.8 ± 0.7 ^k
J02485260-3404246	42.2192	-34.0735	90.2±1.4	-23.7±1.4	Z12	M4(sb1) ^{v, s}	9.31	8.63	8.40	8.25	8.05	14.6 ± 0.3
J02564708-6343027	44.1962	-63.7174	67.4±2.2	8.3±5.6	Z12	M4	11.31 ⁱ	9.86	9.22	9.01	8.80	18.5 ± 3.4
J03050976-3725058	46.2907	-37.4183	50.8±1.3	-12.2±1.3	Z12	M1.5+M3 ^c	11.46	9.54	8.88	8.65	8.46	14.3 ± 0.6
J03350208+2342356	53.7587	23.7099	54.0±10.0	-56.0±10.0	F16	M8.5 ^t	12.25	11.65	11.26	11.06	10.77	15.5 ± 1.7 ^{dd}
J03494535-6730350	57.4390	-67.5097	41.8±1.0	20.5±1.0	Z12	K7	11.16	9.85	9.23	9.03	8.88	16.8 ± 0.2
J04082685-7844471	62.1119	-78.7464	54.7±1.4	42.1±1.4	Z12	M0	10.89	9.28	8.59	8.40	8.26	16.4 ± 0.4
J04091413-4008019	62.3089	-40.1339	45.9±1.7	7.2±1.7	Z12	M3.5	12.82	10.65	10.00	9.77	9.52	21.3 ± 0.5
J04213904-7233562	65.4127	-72.5656	62.2±1.3	26.6±1.3	Z12	M2.5	11.82	9.87	9.25	8.99	8.79	15.0 ± 0.3
J04240094-5512223	66.0040	-55.2062	42.4±2.1	17.2±2.1	Z12	M2.5	11.75	9.80	9.16	8.95	8.80	20.1 ± 0.5
J04363294-7851021	69.1373	-78.8506	33.0±3.0	47.0±2.7	Z12	M4	12.52 ⁱ	10.98	10.36	10.10	9.96	26.5 ± 0.3
J04365738-1613065	69.2391	-16.2185	109.8±3.0	-21.9±4.2	Z12	M3.5	11.30	9.12	8.47	8.26	8.14	15.7 ± 0.5
J04402325-0530082	70.0969	-5.5023	320.4±10.6	126.8±7.3	2MAW	M7 ^e	10.66	9.99	9.55	9.36	9.17	29.9 ± 0.2 ^{dd}
J04433761+0002051	70.9067	0.0348	28.0±14.0	-99.0±14.0	F16	M9 γ^f	12.51	11.80	11.22	10.83	10.48	17.0 ± 0.8 ^k
J04440099-6624036	71.0041	-66.4010	51.6±2.6	33.3±2.6	Z12	M0.5	11.05	9.47	8.75	8.58	8.47	16.7 ± 0.4
J04480066-5041255	72.0028	-50.6904	53.1±2.1	15.7±2.3	Z12	K7	10.42	8.74	8.08	7.92	7.79	19.3 ± 0.1

Table 1. continued

2MASS Designation	Coordinates		Proper Motion		Ref. ^b	Sp.Type ^{a,b} (Opt.)	Magnitudes				Trigonometric distance ^b		Radial Velocity ^b (km s ⁻¹)
	α (J2000.0)	δ (J2000.0)	$\mu_{\alpha} \cos \delta$ (mas yr ⁻¹)	μ_{δ} (mas yr ⁻¹)			J	H	K_S	$W1$	$W2$	(pc)	
J04533054-5551318	73.3773	-55.8588	134.5 ± 2.4	72.7 ± 2.0	vL07	M3Ve+M3Ve ^r	7.80	7.24	6.89	5.96	5.38	11.1 ± 0.2 ^{ff}	30.0 ± 0.0 ^{ee}
J04571728-0621564	74.3220	-6.3657	22.9 ± 1.9	-99.1 ± 2.5	Z12	M0.5	9.51	8.83	8.64	8.53	8.51		23.4 ± 0.3
J04593483+0147007	74.8951	1.7835	34.6 ± 2.3	-94.3 ± 1.4	vL07	M0Ve ^r	7.12	6.45	6.26	6.21	6.06	25.9 ± 1.7 ^{ff}	19.8 ± 0.0 ^b
J05090356-4209199	77.2649	-42.1555	26.7 ± 1.8	59.0 ± 1.4	Z12	M3.5	9.58	8.98	8.76	8.60	8.43		16.8 ± 1.7
J05100427-2340407	77.5178	-23.6780	41.4 ± 2.3	-13.3 ± 1.1	Z12	M3.5+M3.5	9.24	8.58	8.36	8.21	8.06		24.3 ± 0.3
J05142878-1514546	78.6199	-15.2485	34.2 ± 3.3	-13.1 ± 3.4	Z12	M3.5	10.95	10.40	10.10	9.98	9.82		21.4 ± 0.3
J05241317-2104427	81.0549	-21.0786	33.3 ± 2.5	-17.1 ± 2.2	Z12	M4	10.21	9.60	9.32	9.23	9.05		24.5 ± 0.3
J05241914-1601153	81.0798	-16.0209	16.0 ± 2.5	-34.8 ± 3.5	Z12	M4.5+M5.0	8.67	8.13	7.81	7.62	7.42		17.5 ± 0.6
J05254166-0909123	81.4236	-9.1534	39.2 ± 8.0	-188.4 ± 8.0	Z12	M3.8+M5 ^{dd}	10.58	7.88	7.62	7.45	7.30	20.7 ± 2.2 ^{dd}	26.3 ± 0.3
J05332558-5117131	83.3566	-51.2870	43.8 ± 2.1	25.1 ± 2.1	Z12	K7	10.62	8.99	8.36	8.16	8.06		19.6 ± 0.4
J05335981-0221325	83.4992	-2.3590	12.3 ± 1.2	-61.3 ± 2.4	Z12	M3	10.57	7.88	7.70	7.53	7.43		20.9 ± 0.2
J05392505-4245211	84.8544	-42.7559	40.8 ± 1.3	17.5 ± 1.9	Z12	M2	11.34	8.80	8.60	8.47	8.38		21.9 ± 0.2
J05395494-1307598	84.9789	-13.1333	20.3 ± 4.8	-11.7 ± 5.4	Z12	M3	12.62	10.60	9.98	9.72	9.48		24.9 ± 0.4
J05470650-3210413	86.7771	-32.1782	23.7 ± 0.9	7.1 ± 1.7	Z12	M2.5	9.86	9.22	9.03	8.92	8.79		21.9 ± 0.6
J05575096-1359503	89.4624	-13.9973	0.0 ± 5.0	0.0 ± 5.0	F16	M7 ^{dd}	12.87	12.15	11.73	11.24	10.60		30.3 ± 2.8 ^{dd}
J06045215-3433360	91.2173	-34.5600	27.3 ± 0.3	340.9 ± 0.3	Rh11	M5 ^r	7.74	7.18	6.87	6.67	6.39	8.4 ± 0.1 ^x	22.4 ± 0.3 ^x
J06085283-2753583	92.2201	-27.8995	8.9 ± 3.5	10.7 ± 3.5	F16	M8.5e ^f	13.60	12.90	12.37	11.98	11.62	31.3 ± 3.5 ^j	24.0 ± 1.0 ^w
J06112997-7213388	92.8749	-72.2274	23.2 ± 1.6	60.2 ± 1.7	Z12	M4+M5	9.55	8.96	8.70	8.55	8.36		18.2 ± 2.0
J06131330-2742054	93.3055	-27.7015	-13.1 ± 1.6	-0.3 ± 1.3	Z12	M3.5	8.00	7.43	7.14	7.01	6.82	29.4 ± 0.9 ^y	22.5 ± 0.2
J06434332-6424396	100.9388	-64.4110	1.6 ± 2.4	53.1 ± 2.4	Z12	M3+M4+M5	9.29	8.59	8.37	8.24	8.09		20.2 ± 0.4
J08173943-8243298	124.4143	-82.7249	-80.3 ± 1.1	102.5 ± 0.8	Z12	M3.5+	7.47	6.84	6.59	6.48	6.27		15.6 ± 1.5
J08471906-5717547	131.8294	-57.2985	-123.0 ± 1.2	12.3 ± 1.2	Z12	M4	11.57	9.41	8.81	8.55	8.37		30.2 ± 0.2
J10260210-4105537	156.5088	-41.0983	-45.3 ± 1.4	-2.5 ± 1.4	Z12	M0.5	9.18	8.49	8.27	8.15	8.06		
J10285555+0050275	157.2315	0.8410	-603.8 ± 1.9	-728.9 ± 2.0	vL07	M2V ^r	6.18	5.61	5.31	5.18	4.87	7.07 ± 0.03 ^{ff}	8.3 ± 0.5 ^m
J11115267-4401538	167.9695	-44.0316	-22.0 ± 2.0	-12.0 ± 4.0	Z05	M3.9 ^{cc}	12.09	11.49	11.22	11.10	10.91		17.6 ± 0.3 ^{cc}
J11305355-4628251	172.7231	-46.4737	-35.3 ± 2.2	4.7 ± 1.8	Z12	M2.4 ^{cc}	14.13	12.09	11.57	11.29	10.99		10.0 ± 0.1 ^{cc}
J11592786-4510192	179.8661	-45.1720	-52.8 ± 5.1	-12.8 ± 2.8	Z12	M4.5 ^z	11.53 ⁱ	9.93	9.35	9.06	8.72		
J12210499-7116493	185.2708	-71.2804	-42.7 ± 1.8	-10.2 ± 1.6	Z12	K7	10.57	9.09	8.42	8.24	8.17		13.5 ± 0.3
J12265135-3316124	186.7140	-33.2701	-54.0 ± 5.9	-35.0 ± 6.3	2MAW	M6.3 ^{cc}	13.44	10.69	10.12	9.78	9.57	15.1 ± 0.7 ^h	
J12300521-4402359	187.5217	-44.0433	-56.8 ± 7.0	-12.8 ± 1.9	Z12	M4 ^z	12.65	10.45	9.84	9.57	9.26		
J12383713-2703348	189.6547	-27.0597	-185.1 ± 5.1	-185.2 ± 5.1	Ro10	M2.5+	10.57	8.73	8.08	7.84	7.57		9.9 ± 0.2
J14284804-7430205	217.2002	-74.5057	-61.6 ± 1.7	-34.6 ± 1.7	Z12	M1V ^d	11.07	9.26	8.57	8.35	8.21		11.0 ± 0.6
J14361471-7654534	219.0613	-76.9149	-45.0 ± 1.9	-17.4 ± 1.9	Z12	M0.5	11.69	9.84	9.17	8.96	8.75		
J15244849-4929473	231.2021	-49.4965	-120.8 ± 8.0	-241.0 ± 8.0	Z12	M2	9.45 ⁱ	8.16	7.53	7.30	7.14	7.02	10.3 ± 0.2
J15310958-3504571	232.7899	-35.0825	-20.6 ± 2.0	-25.4 ± 2.0	Z12	M4.5 ^z	12.40 ⁱ	10.72	10.10	9.80	9.63	9.40	
J16430128-1754274	250.7554	-17.9076	-26.6 ± 1.2	-52.4 ± 1.3	Z12	M0.5	11.18	9.44	8.76	8.55	8.44		-9.3 ± 0.4

Table 1. *continued*

2MASS Designation	Coordinates		Proper Motion		Sp.Type ^{a,b} (Opt.)	Magnitudes					Trigonometric distance ^b (pc)	Radial Velocity ^b (km s ⁻¹)	
	α (J2000.0)	δ (J2000.0)	$\mu_{\alpha} \cos \delta$ (mas yr ⁻¹)	μ_{δ} (mas yr ⁻¹)		Ref. ^b	J	H	K_S	W1			W2
J16572029-5343316	254.3346	-53.7255	-13.0±6.3	-85.1±2.2	Z12	M3	10.61	8.69	8.07	7.79	7.68	7.57	1.4±0.2
J18420694-5554254	280.5290	-55.9071	9.7±12.1	-81.2±2.8	Z12	M3.5	11.61	9.49	8.82	8.58	8.49	8.33	0.3±0.5
J19225071-6310581	290.7113	-63.1828	-7.9±16.7	-77.5±1.9	Z12	M3	11.41	9.45	8.82	8.58	8.43	8.29	6.4±1.5
J19355595-2846343	293.9832	-28.7762	34.0±12.0	-58.0±12.0	F16	M9 γ^k		13.95	13.18	12.71	12.38	11.90	
J19560294-3207186	299.0123	-32.1219	35.2±1.8	-59.9±1.5	Z12	M4+	11.03	8.96	8.34	8.11	7.92	7.76	-3.7±2.2
J20004841-7523070	300.2018	-75.3853	69.0±12.0	-110.0±4.0	F16	M9 ^{bb}		12.73	11.97	11.51	11.13	10.81	4.4±2.8 ^k
J20013718-3313139	300.4049	-33.2206	27.0±3.2	-58.6±2.0	Z12	M1	10.85	9.15	8.46	8.24	8.16	8.09	-3.7±0.2
J20100002-2801410	302.5001	-28.0281	40.7±3.0	-62.0±1.7	Z12	M2.5+M3.5	10.92	8.65	8.01	7.73	7.61	7.45	-5.8±0.6
J20333759-2556521	308.4066	-25.9478	52.8±1.7	-75.9±1.3	Z12	M4.5	12.42	9.71	9.15	8.88	8.68	8.44	-7.6±0.4
J20465795-0259320	311.7415	-2.9922	53.0±2.5	-109.5±1.7	Z12	M0	10.75	9.12	8.44	8.27	8.24	8.22	-14.2±0.3
J21100535-1919573	317.5223	-19.3326	89.0±0.9	-89.9±1.8	Z12	M2	10.07	8.11	7.45	7.20	7.02	7.00	-5.7±0.4
J21265040-8140293	321.7100	-81.6748	55.6±1.4	-101.8±3.0	F16	L3 γ^g	15.54	14.40	13.55	12.93	12.47	12.47	10.0±0.5 ^k
J21471964-4803166	326.8318	-48.0546	50.9±1.7	-74.0±2.0	Z12	M4	13.08	10.73	10.19	9.92	9.75	9.60	10.4±2.9
J21521039+0537356	328.0433	5.6266	128.1±7.0	-135.6±26.7	2MAW	M2Ve ^r	9.75 ^{gg}	8.25	7.65	7.39	7.14	7.07	-15.1±1.5 ^{dd}
J22021626-4210329	330.5677	-42.1758	50.4±1.0	-90.9±1.5	Z12	M1	10.72	8.93	8.23	7.99	7.89	7.87	-2.6±0.5
J22440873-5413183	341.0364	-54.2218	70.7±1.3	-60.0±1.3	Z12	M4+	11.51	9.36	8.71	8.47	8.30	8.14	1.6±1.6
J22470872-6920447	341.7863	-69.3458	70.9±1.6	-58.9±1.8	Z12	K7(sbl) ^{v,s}	10.37	8.89	8.30	8.09	8.01	8.00	17.3±0.2
J23131671-4933154	348.3196	-49.5543	77.5±2.1	-88.1±1.7	Z12	M4	12.07	9.76	9.14	8.92	8.77	8.58	1.9±0.3
J23221088-0301417	350.5453	-3.0283	92.4±1.6	-68.3±1.7	Z12	K7	10.44	8.73	8.12	7.93	7.85	7.89	-5.4±0.3
J23285763-6802338	352.2402	-68.0427	66.8±1.9	-67.1±1.7	Z12	M2.5	11.27	9.26	8.64	8.38	8.27	8.16	10.8±3.4
J23301341-2023271	352.5559	-20.3909	311.8±3.2	-207.4±3.0	vL07	M3(sb2) ^{v,ee}	9.02 ^{ff}	7.20	6.61	6.33	6.23	6.02	-5.7±0.8
J23320018-3917368	353.0008	-39.2936	193.4±17.9	-178.4±17.9	Ro10	M3	11.08	8.90	8.26	8.02	7.88	7.75	11.1±0.2
J23452225-7126505	356.3427	-71.4474	80.3±2.2	-62.4±2.1	Z12	M3.5	12.40	10.19	9.57	9.32	9.17	8.98	8.6±0.3
J23474694-6517249	356.9456	-65.2903	79.2±1.2	-66.8±1.2	Z12	M1.5	10.88	9.10	8.39	8.17	8.09	8.02	6.2±0.5

^aThe symbols β and γ are used when referring to Allers & Liu (2013) INT-G and VL-G gravity classes, for simplicity.

^bReferences : Spectral type references from Riaz et al. (2006) unless otherwise stated. I magnitude from Zacharias et al. (2012) unless otherwise stated. Radial velocities from Malo et al. (2014a) unless otherwise stated. (a) Anderson & Francis 2012, (b) Bailey et al. 2012, (c) Bergfors et al. 2010, (d) Bowler et al. 2015, (e) Cruz et al. 2003, (f) Cruz et al. 2007, (g) Cruz et al. 2009, (h) Donaldson et al., in prep., (i) Epchein et al. 1997, (j) Faherty et al. 2012, (k) Faherty et al. 2016, (l) Gagné (2017, private communication), (m) Gontcharov 2006, (n) Jansson et al. 2012, (o) Kirkpatrick et al. 2010, (p) Kiss et al. 2011, (q) Koen et al. 2010, (r) Malo et al. 2013, (s) Malo et al. 2014a, (t) Reid et al. 2002, (u) Reid et al. 2008, (v) Riaz et al. 2006, (w) Rice et al. 2010, (x) Riedel et al. 2011, (y) Riedel et al. 2014, (z) Rodriguez et al. 2011, (aa) Roeser et al. 2010, (bb) Schmidt et al. 2007, (cc) Shkolnik et al. 2011, (dd) Shkolnik et al. 2012, (ee) Torres et al. 2006, (ff) van Leeuwen 2007, (gg) Weis 1991, (hh) Zacharias et al. 2005, (ii) Zacharias et al. 2012, (F16) Faherty et al. 2016, (Ri11) Riedel et al. 2011, (Ro10) Roeser et al. 2010, (Z05) Zacharias et al. 2005, (Z12) Zacharias et al. 2012, (vL07) van Leeuwen 2007, (2MAW) Measured from 2MASS and WISE.

Table 2. Sample Age and Distance

2MASS designation	Status ^a	Adopted Age Range ^b (Myr)		constraints	Adopted Distance Range ^c (pc)		source
		min	max		min	max	
J00040288-6410358	HLC	41	49	THA	43	49	d_s ; THA
J00172353-6645124	HLC	21	27	BPMG	36	41	π ; Riedel et al. 2014
J00325584-4405058	AY	41	200	THA; ABDMG	30	61	π ; Faherty et al. 2016
J00374306-5846229	YO	5	200	YO	38	60	d_{sp}
J01071194-1935359	YO	21	200	YO; Li	13	69	d_s ; BPMG; COL; FIELD
J01123504+1703557	HLC	130	200	ABDMG	45	49	d_s ; ABDMG
J01132958-0738088	YO	5	1000	YO; H α	39	59	d_s ; FIELD
J01220441-3337036	HLC	41	49	THA	37	41	d_s ; THA
J01351393-0712517	AY	21	48	COL; BPMG	35	40	π ; Shkolnik et al. 2012
J01415823-4633574	HLC	41	49	THA	37	42	d_s ; THA
J01484087-4830519	HLC	130	200	ABDMG	34	38	d_s ; ABDMG
J01521830-5950168	HLC	41	49	THA	37	41	d_s ; THA
J02045317-5346162	HLC	41	49	THA	39	43	d_s ; THA
J02070176-4406380	HLC	41	49	THA	41	45	d_s ; THA
J02155892-0929121	HLC	41	49	THA	41	45	d_s ; THA
J02215494-5412054	HLC	41	49	THA	36	41	d_s ; THA
J02224418-6022476	HLC	41	49	THA	29	33	d_s ; THA
J02251947-5837295	C	41	49	THA	40	45	d_s ; THA
J02303239-4342232	HLC	38	48	COL	50	54	d_s ; COL
J02340093-6442068	HLC	41	49	THA	42	49	d_s ; THA
J02485260-3404246	AY	38	49	COL; THA	40	46	d_s ; COL; THA
J02564708-6343027	AY	38	49	COL; THA	50	60	d_s ; COL; THA
J03050976-3725058	HLC	38	48	COL	68	76	d_s ; COL
J03350208+2342356	BF	21	27	BPMG	40	44	π ; Shkolnik et al. 2012
J03494535-6730350	HLC	38	48	COL	77	85	d_s ; COL
J04082685-7844471	HLC	38	56	CAR	53	55	d_s ; CAR
J04091413-4008019	HLC	38	48	COL	58	68	d_s ; COL
J04213904-7233562	HLC	41	49	THA	49	57	d_s ; THA
J04240094-5512223	HLC	38	48	COL	62	72	d_s ; COL
J04363294-7851021	HLC	130	200	ABDMG	51	61	d_s ; ABDMG
J04365738-1613065	AY	21	49	THA; BPMG	12	34	d_s ; THA; BPMG
J04402325-0530082	NYI	200	10000	Allers & Liu 2013 ; Cruz et al. 2009	9	9	π ; Riedel et al. 2014
J04433761+0002051	HLC	21	27	BPMG	22	28	d_s ; BPMG
J04440099-6624036	HLC	41	49	THA	50	58	d_s ; THA
J04480066-5041255	HLC	41	49	THA	48	56	d_s ; THA

Table 2. *continued*

2MASS designation	Status ^a	Adopted Age Range ^b (Myr)		constraints		Adopted Distance Range ^c (pc)		source
		min	max	min	max	min	max	
J04533054-5551318	BF	130	200		ABDMG	10	11	π ; van Leeuwen 2007
J04571728-0621564	HLC	130	200		ABDMG	42	48	d_s ; ABDMG
J04593483+0147007	BF	21	27		BPMG	24	27	π ; van Leeuwen 2007
J05090356-4209199	AY	21	50		BPMG; ARG	19	55	d_s ; BPMG; ARG
J05100427-2340407	HLC	38	48		COL	44	54	d_s ; COL
J05142878-1514546	HLC	38	48		COL	54	66	d_s ; COL
J05241317-2104427	HLC	38	48		COL	46	56	d_s ; COL
J05241914-1601153	HLC	21	27		BPMG	14	24	d_s ; BPMG
J05254166-0909123	HLC	130	200		ABDMG	18	22	π ; Shkolnik et al. 2012
J05332558-5117131	HLC	41	49		THA	48	56	d_s ; THA
J05335981-0221325	HLC	21	27		BPMG	30	38	d_s ; BPMG
J05392505-4245211	AY	38	49		COL; THA	37	56	d_s ; COL; THA
J05395494-1307598	HLC	38	48		COL	59	77	d_s ; COL
J05470650-3210413	HLC	38	48		COL	45	59	d_s ; COL
J05575096-1359503	YO	5	400		YO	30	49	d_{ph} ; Shkolnik et al. 2012
J06045215-3433360	BF	30	50		ARG	8	8	π ; ?
J06085283-2753583	YO	5	200		YO	20	32	d_{sep}
J06112997-7213388	HLC	38	56		CAR	45	49	d_s ; CAR
J06131330-2742054	HLC	21	27		BPMG	28	30	π ; Riedel et al. 2014
J06434532-6424396	AY	38	56		CAR; COL	49	59	d_s ; CAR; COL
J08173943-8243298	HLC	21	27		BPMG	25	29	d_s ; BPMG
J08471906-5717547	HLC	130	200		ABDMG	20	24	d_s ; ABDMG
J10260210-4105537	C	7	13		TWA	56	66	d_s ; TWA
J10285555+0050275	BF	130	200		ABDMG	7	7	π ; van Leeuwen 2007
J11115267-4401538	YO	90	160		Shkolnik et al. 2011	27	40	d_{ph} ; Shkolnik et al. 2011
J11305355-4628251	YO	20	130		Shkolnik et al. 2011	49	74	d_{ph} ; Shkolnik et al. 2011
J11592786-4510192	YO	5	12		ScoCen; Rodriguez et al. 2011	44	66	d_{ph} ; Rodriguez et al. 2011
J12210499-7116493	YO	3	15		Kiss et al. 2011	88	107	d_{kin} ; Kiss et al. 2011
J12265135-3316124	BF	7	13		TWA	63	69	π ; Donaldson et al. 2016
J12300521-4402359	YO	5	12		ScoCen; Rodriguez et al. 2011	55	82	d_{ph} ; Rodriguez et al. 2011
J12383713-2703348	HLC	130	200		ABDMG	22	24	d_s ; ABDMG
J14284804-7430205	YO	21	1000		No Li; Malo (2017, in preparation); Ho; Riaz et al. 2006	24	68	d_s ; BPMG; CAR; FIELD
J14361471-7654534	YO	21	1000		No Li; Malo (2017, in preparation); Ho; Riaz et al. 2006	26	44	d_s ; FIELD
J15244849-4929473	HLC	130	200		ABDMG	23	25	d_s ; ABDMG
J15310958-3504571	YO	5	12		ScoCen; Rodriguez et al. 2011	56	84	d_{ph} ; Rodriguez et al. 2011
J16430128-1754274	YO	21	200		Li; Malo (2017, in preparation)	31	51	d_s ; FIELD
J16572029-5343316	HLC	21	27		BPMG	49	55	d_s ; BPMG

Table 2. *continued*

2MASS designation	Status ^a	Adopted Age Range ^b (Myr)		Adopted Distance Range ^c (pc)		source	
		min	max	min	max		
J18420694-5554254	HLC	21	27	BPMG	49	57	d_s ; BPMG
J19225071-6310581	AY	21	49	BPMG; THA	49	66	d_s ; BPMG; THA
J19355595-2846343	YO	5	200	YO	24	38	d_{sp}
J19560294-3207186	HLC	21	27	BPMG	54	62	d_s ; BPMG
J20004841-7523070	HLC	21	27	BPMG	28	35	d_s ; BPMG
J20013718-3313139	HLC	21	27	BPMG	58	66	d_s ; BPMG
J20100002-2801410	HLC	21	27	BPMG	44	51	π ; Riedel et al. 2014
J20333759-2556521	HLC	21	27	BPMG	44	51	π ; Riedel et al. 2014
J20465795-0259320	HLC	130	200	ABDMG	44	48	d_s ; ABDMG
J21100535-1919573	HLC	21	27	BPMG	31	35	d_s ; BPMG
J21265040-8140293	YO	5	200	YO	29	34	π ; Faherty et al. 2016
J21471964-4803166	AY	21	200	ABDMG; BPMG; THA	41	69	d_s ; ABDMG; BPMG; THA
J21521039+0537356	BF	130	200	ABDMG	25	35	π ; van Leeuwen 2007
J22021626-4210329	HLC	41	49	THA	43	49	d_s ; THA
J22440873-5413183	HLC	41	49	THA	45	51	d_s ; THA
J22470872-6920447	HLC	130	200	ABDMG	52	58	d_s ; ABDMG
J23131671-4933154	HLC	41	49	THA	38	42	d_s ; THA
J23221088-0301417	YO	10	1000	YO; H α	30	46	d_s ; COL; BPMG
J23285763-6802338	HLC	41	49	THA	45	51	d_s ; THA
J23301341-2023271	HLC	38	48	COL	15	17	π ; van Leeuwen 2007
J23320018-3917368	HLC	130	200	ABDMG	22	24	d_s ; ABDMG
J23452225-7126505	HLC	41	49	THA	42	48	d_s ; THA
J23474694-6517249	HLC	41	49	THA	44	48	d_s ; THA

^aStatus: BF: bona fide; HLC: high-likelihood candidate, unambiguous membership (high probability considering radial velocity or parallax measurements); C: Candidate (high probability without RV or plx confirmation); AY: ambiguous young (more than one association has a high probability); YO: other young stars; NYI: no youth indicator.

^bFor high-likelihood candidates and stars with ambiguous membership, the total range of the association(s) is given.

^cAdopted distance range source: d_s : statistical distance; d_{ph} : photometric distance; d_{sp} : spectrophotometric distance; dkin: kinematic distance; π : parallax.

mass companions, the only objects that have such colors are field L/T dwarfs and the much rarer high-redshift quasars (Delorme et al. 2008; Reyl e et al. 2010). Field L/T dwarfs are rare. Allen et al. (2005) have estimated a local density of L dwarfs ($M_J=11.75\text{--}14.75$) to be $7.35 \times 10^{-3} \text{pc}^{-3}$, while Reyl e et al. (2010) estimated the local density of T0–T5.5 dwarfs to be $1.4 \times 10^{-3} \text{pc}^{-3}$. Within a 5'5 FOV and a maximum distance of 100 pc, each field samples $\sim 0.85 \text{pc}^3$. For the entire survey (81pc^3), that amounts to ~ 0.6 L dwarfs and ~ 0.11 early-T. Less than one such false positive was therefore expected. An astrometric follow-up can be made to confirm common proper motion to the primary and eliminate these false positives. Host stars in the present sample are nearby and in general have high proper motions. Common proper motion can be detected within at most a few years for all targets. The dashed line in Figure 4 indicates the approximate limit above which objects are also detected in the 2MASS catalog (Cutri et al. 2003), calculated using typical $z'-J$ colors (Zhang et al. 2009) and the $J < 16$ limit of 2MASS. The earliest candidates can thus be readily identified as comoving with the primary, because 2MASS observations were taken ~ 10 years earlier. High-redshift quasars are even rarer per unit surface at a given apparent magnitude and can be distinguished with broadband NIR photometry. Their flux is not rising toward the infrared (their red color in $i' - z'$ is due to the Lyman forest absorption blueward of the $\text{Ly}\alpha$ emission line), and they have much more neutral $z'-J$ colors than substellar companions and would not display common proper motion with the nearby star. Optical and mid-infrared (*WISE*) colors can also help to distinguish those.

Candidates warmer than $\sim \text{T2}$ are detected in both the i' and z' -bands, while cooler objects down to $\sim \text{T4}$ are detected as i' -dropouts (dark and light cyan regions, respectively, on Figure 3). Note that the i' and z' observations are optimal to identify late-L to early-T companions, which at the young age of the stars in the survey are planetary-mass or low-mass brown dwarfs. Contrary to what would be the case for standard high-contrast imaging surveys, this survey is much *less* sensitive to earlier-L or late-M, which have less distinctive $i' - z'$. The focus here is thus on planetary-mass companions and not on brown dwarfs.

The observations allow us to detect companions as close as $5''\text{--}70''$ to the target (depending on its brightness) and up to the edge of the GMOS 5'5 field of view ($\sim 165''$ from the target). For a typical target at 45 pc, this allows to survey a distance of ~ 7400 au. We chose to limit our analysis to 5000 au to be complete for most of the targets of the survey and because it corresponds to the observed upper limit on the separation of low-mass stellar binaries (Artigau et al. 2007; Caballero et al.

2007; Radigan et al. 2009; Dhital et al. 2010).

3.2. Observations

The observations were carried out in 2011–2012 at Gemini South during three different semesters (see Table 3). Broadband imaging was performed with GMOS in the i' (iG0327, 700–850 nm) and z' (zG0328, >850 nm) filters. The GMOS detector is made of three 2048×4608 CCDs, with a pixel scale of $0''.073/\text{pixel}$, for a total field of view of 5'5 squared. In each band, at least three exposures were taken, with a small dither between each, in order to remove cosmic rays and fill the gaps between the detectors. The exposure time in z' (200 s per individual exposure) was chosen to reach $z = 22$, the apparent magnitude of an $M_z = 18$ object for the most distant targets in the sample (~ 80 pc). This allows us to detect objects down to a temperature of about 900 K (T5). In the i' band, individual exposures of 300 s were obtained in order to reach $i'=24.5$ and thus minimally detect objects with $i' - z'=2.5$ ($\sim \text{L6}$). This constraint on $i' - z'$ minimizes the number of false positives and thus the follow-up time. Observations in the i' and z' bands were scheduled together when possible, in order to lower the overall time required per observation and reduce the likelihood of astrophysical false positives from variable objects. Observations in both filters typically required ~ 36 minutes per target, including overheads. A summary of observations for individual targets is shown in Table 4.

Table 3. Observing Log

Program no.	Dates	Total Time (hr)	Targets observed
GS-2011B-Q-74	2011 Aug.–Oct.2	22	34
GS-2012A-Q-78	2012 Feb.–Jul.	22.2	27
GS-2012B-Q-75	2012 Jul.–2013 Jan.	20.9	34

3.3. Data Reduction

A custom data-reduction pipeline was used to process GMOS i' and z' images. Each i' or z' image is composed of three files that correspond to the three 2048×4608 chips of the GMOS detector. After making a basic reduction, including the identification of bad pixels and saturated pixels, overscan and bias subtraction, fringe correction and flat-field division, the astrometry of each portion was independently anchored to the USNO-B1 catalog. The positions of the left and right chips relative to the middle one were then computed for all images using reference points. The median relative position was adopted, and the final i' or z' images were reconstructed.

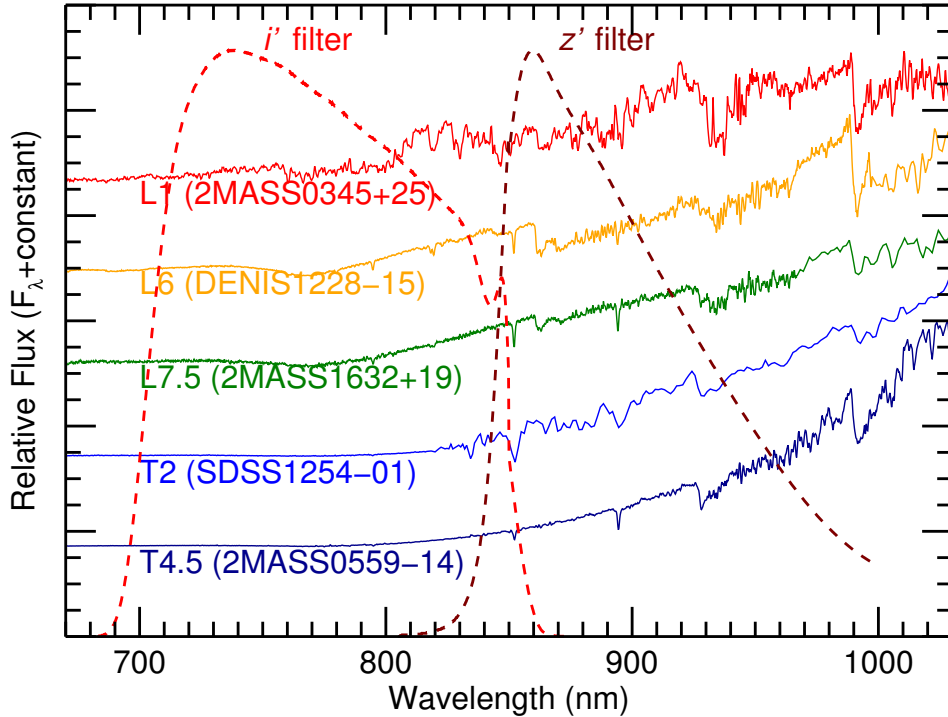


Figure 3. The far-red spectra of five objects with spectral types ranging from early-Ls to mid-Ts (from the L and T dwarf data archive; <http://staff.gemini.edu/~sleggett/LTdata.html>). The spectra are normalized at 960 nm and offset for clarity. The transmission curves of the GMOS i' and z' filters (similar to SDSS filters) are superimposed. The z' filter curve includes the response from the detector.

For each star and each filter, three or more images were taken. As optimal photometric conditions were not requested for the observations, the transmission sometimes varied significantly during exposures. The maximal cloud cover requested (CC=70%) implies patchy clouds or extended thin cirrus clouds that lead to a maximum loss of 0.3 mag¹. Images with a transmission below 70% of the best case were rejected. If there were more than three images satisfying this condition, all images with a measured FWHM no larger than 1.2 times that of the third best were kept (to avoid adding images with a good transmission but taken under bad seeing). For all stars and in both filters, there were always at least two images remaining. All images were scaled to match the zero point of the highest-throughput image before median-combining them to obtain a deep image for each filter. Table 4 lists, for each object, the number of images that were considered and the FWHM of the combined image produced. The FWHM varies between

0''.5 and 1''.6 in both filters, with a median of 1''.0.

3.4. Assessment of conditions and photometric calibration

One significant challenge in analyzing nonphotometric observations is to flux-calibrate the data. It is useful first to identify which observations were likely taken under photometric conditions and which were not. This can be done by looking at the variation of the transmission in the three i' or z' images. If the rms of the transmission of consecutive retained images was more than 3%, the conditions were suspected to be nonphotometric. The fields with nonphotometric conditions were identified with the mention “light clouds” (lc) in Table 4. The other were assumed to have been taken under almost photometric conditions (phot). It is possible, although unlikely, that a nonnegligible cloud cover remained stable over a ~ 20 minutes of observation. That would lead to a slight underestimation of the error on the zero points in those cases. The effect on the results of the survey is however negligible.

When available, the zero point was determined through a cross-match with the Sloan Digital Sky Sur-

¹ <http://www.gemini.edu/sciops/telescopes-and-sites/observing-condition-constraints>

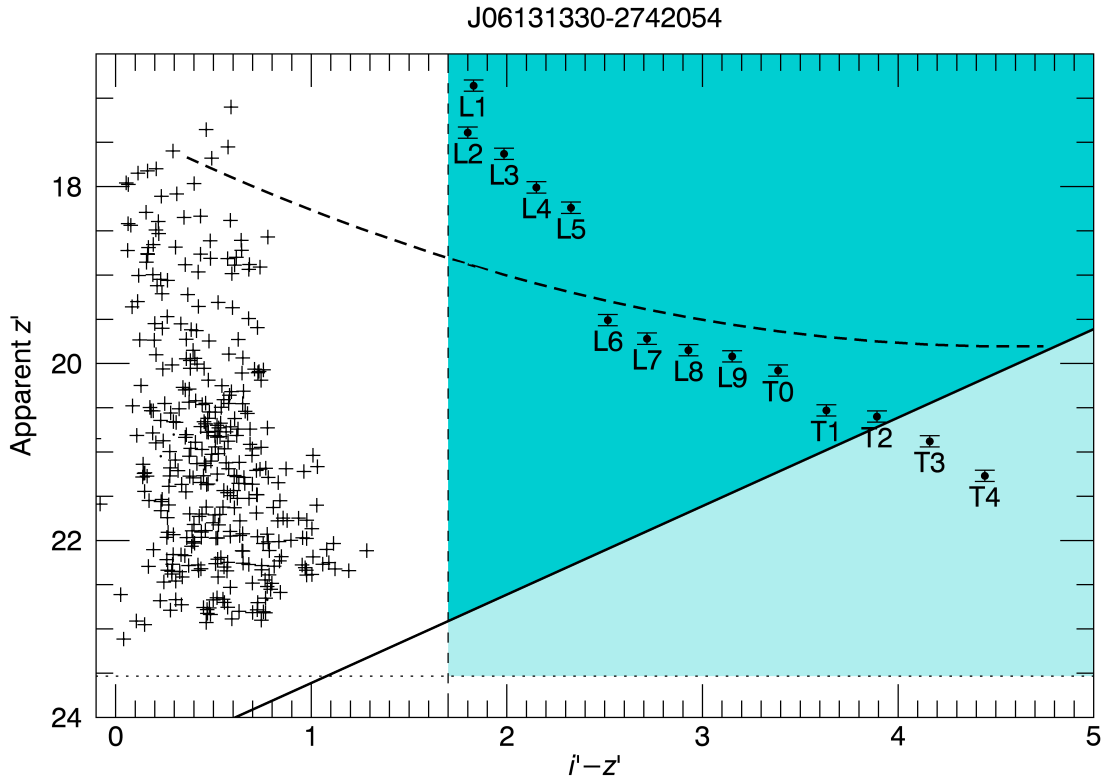


Figure 4. Color-magnitude diagram for all objects present in the field of a typical target of the survey. Also shown are fields L0–T4 at the range of distance of the target (West et al. 2005; Zhang et al. 2009). Younger objects with inflated radii would appear higher (brighter) on this figure. There are 353 objects identified in this field, but none with an $i' - z' \gtrsim 1.3$. Objects in the dark cyan region are detected in both the i' and z' -band while cooler objects, down to T4, are detected as i' -dropouts (light cyan region). The dashed line indicates the approximate limit above which objects are also detected in 2MASS ($J < 16$, earlier than L5).

vey (SDSS DR9; Ahn et al. 2012). Other fields were flux-calibrated using the SkyMapper (Wolf et al. 2016) early data release² or the Pan-STARRS (Schlafly et al. 2012; Magnier et al. 2013) PV3 release. SkyMapper and Pan-STARRS magnitudes were first converted to SDSS magnitudes using, respectively, the procedure explained on the web site³ and the color correction from Tonry et al. (2012). For each field, point sources are then identified in the calibrated survey field and in that of GMOS. The zero point adopted for each field and filter is the median of the zero points computed for each source, which is the difference between the cataloged magnitude and that computed in the GMOS field. The errors for the zero points computed this way are taken to be the standard deviation of the zero points computed for every source divided by the square root of the number of sources (typically < 0.05). The medians of zero points obtained from the three surveys are in agreement. The computed zero points for the different fields

vary between 26.5 and 27.1 with a median of 26.8 in i' and between 25.2 and 26 with a median of 25.7 in z' (see Table 4).

About one-half of the 95 fields are not found in SDSS, Pan-STARRS or SkyMapper and cannot be directly calibrated. For these, the median of the values found for the calibrated fields was assigned. The calibrated fields that were identified non photometric were not used in the computation of this median. An error of 0.15 or 0.25 was conservatively assigned on the zero point assigned this way for observations taken under photometric conditions and nonphotometric conditions, respectively, given the dispersion of the zero points for the fields that were calibrated. This is consistent with the computed $\Delta(ZP_{\text{computed}} - ZP_{\text{median}})$ for the fields for which the zero point was computed and is also compatible with the expected maximal loss of flux under a CC of 70%.

² <http://skymapper.anu.edu.au/data-release/>

³ <http://skymapper.anu.edu.au/filter-transformations/>

Table 4. Summary of individual target observations

Name	Filter	Obs. Date(s; UT) (YYYYMMDD)	N_{exp}	Condition ^a	FWHM "	Zero point	Source ^b
J00040288-6410358	<i>i</i>	20120920	3	phot	0.9	26.87± 0.15	med
	<i>z</i>	20120920	3	lc	0.8	25.75± 0.25	med
J00172353-6645124	<i>i</i>	20110804	3	phot	1.2	26.87± 0.15	med
	<i>z</i>	20110804	3	phot	1.1	25.75± 0.15	med
J00325584-4405058	<i>i</i>	20120921	3	phot	1.4	26.87± 0.15	med
	<i>z</i>	20120921	4	phot	1.3	25.75± 0.15	med
J00374306-5846229	<i>i</i>	20120920	3	phot	1.1	26.87± 0.15	med
	<i>z</i>	20120920	3	lc	1.1	25.75± 0.25	med
J01071194-1935359	<i>i</i>	20111006	3	phot	1.4	27.00± 0.07	PS
	<i>z</i>	20111006	3	lc	1.1	26.03± 0.07	PS
J01123504+1703557	<i>i</i>	20110922,20111018	7	phot	1.1	26.87± 0.01	SDSS
	<i>z</i>	20110922,20111018	3	phot	1.0	25.73± 0.02	SDSS
J01132958-0738088	<i>i</i>	20111007	3	phot	1.4	27.04± 0.03	SDSS
	<i>z</i>	20111007	3	phot	1.3	25.86± 0.02	SDSS
J01220441-3337036	<i>i</i>	20111005	3	phot	1.6	26.87± 0.15	med
	<i>z</i>	20111005	3	phot	1.5	25.75± 0.15	med
J01351393-0712517	<i>i</i>	20110922	3	phot	1.2	27.01± 0.02	SDSS
	<i>z</i>	20110922	3	phot	1.1	25.88± 0.04	SDSS
J01415823-4633574	<i>i</i>	20120915	3	phot	1.3	26.87± 0.15	med
	<i>z</i>	20120915	3	lc	1.2	25.75± 0.25	med
J01484087-4830519	<i>i</i>	20111006	3	phot	1.2	26.91± 0.04	SM
	<i>z</i>	20111006	3	phot	1.1	25.79± 0.05	SM
J01521830-5950168	<i>i</i>	20120203	3	phot	1.1	26.87± 0.15	med
	<i>z</i>	20120203	3	phot	1.1	25.75± 0.15	med
J02045317-5346162	<i>i</i>	20110804	3	phot	1.2	26.87± 0.15	med
	<i>z</i>	20110804	3	phot	1.1	25.75± 0.15	med
J02070176-4406380	<i>i</i>	20110921	3	lc	0.9	26.51± 0.05	SM
	<i>z</i>	20110921	3	lc	0.8	25.64± 0.03	SM
J02155892-0929121	<i>i</i>	20111007	3	phot	1.6	26.91± 0.02	SDSS
	<i>z</i>	20111007	3	phot	1.4	25.73± 0.04	SDSS
J02215494-5412054	<i>i</i>	20120827	3	lc	0.9	26.87± 0.25	med
	<i>z</i>	20120827	3	lc	0.9	25.75± 0.25	med
J02224418-6022476	<i>i</i>	20110916	3	phot	1.3	26.87± 0.15	med
	<i>z</i>	20110916	3	phot	1.2	25.75± 0.15	med
J02251947-5837295	<i>i</i>	20120826	3	phot	1.6	26.87± 0.15	med
	<i>z</i>	20120826	3	phot	1.6	25.75± 0.15	med
J02303239-4342232	<i>i</i>	20120730	3	phot	1.1	26.87± 0.15	med
	<i>z</i>	20120730	3	phot	0.8	25.75± 0.15	med
J02340093-6442068	<i>i</i>	20120826	3	phot	1.2	26.78± 0.04	SM
	<i>z</i>	20120826	3	lc	1.3	25.71± 0.03	SM
J02485260-3404246	<i>i</i>	20111006	3	phot	1.1	26.87± 0.15	med
	<i>z</i>	20111006	3	phot	1.0	25.75± 0.15	med
J02564708-6343027	<i>i</i>	20111005	2	phot	1.5	26.87± 0.15	med
	<i>z</i>	20111005	3	phot	1.3	25.75± 0.15	med
J03050976-3725058	<i>i</i>	20111007,20111011	6	phot	1.5	26.97± 0.04	SM
	<i>z</i>	20111007,20111011	3	phot	1.6	25.83± 0.04	SM
J03350208+2342356	<i>i</i>	20130103	3	phot	1.1	26.84± 0.02	PS
	<i>z</i>	20130103	3	phot	1.0	25.70± 0.02	PS

Table 4 continued

Table 4 (*continued*)

Name	Filter	Obs. Date(s; UT) (YYYYMMDD)	N_{exp}	Condition ^a	FWHM "	Zero point	Source ^b
J03494535-6730350	<i>i</i>	20111009	3	phot	0.9	26.87± 0.15	med
	<i>z</i>	20111009	3	phot	0.8	25.75± 0.15	med
J04082685-7844471	<i>i</i>	20111011	3	phot	1.0	26.87± 0.15	med
	<i>z</i>	20111011	3	phot	1.1	25.75± 0.15	med
J04091413-4008019	<i>i</i>	20120827	3	phot	1.3	26.87± 0.15	med
	<i>z</i>	20120827	3	phot	1.3	25.75± 0.15	med
J04213904-7233562	<i>i</i>	20110922	3	phot	1.2	26.87± 0.15	med
	<i>z</i>	20110922	3	phot	1.1	25.75± 0.15	med
J04240094-5512223	<i>i</i>	20110916	3	phot	1.3	26.87± 0.15	med
	<i>z</i>	20110916	3	phot	1.0	25.75± 0.15	med
J04363294-7851021	<i>i</i>	20120915	3	lc	1.3	26.53± 0.02	SM
	<i>z</i>	20120915	3	lc	1.2	25.20± 0.02	SM
J04365738-1613065	<i>i</i>	20111008	3	phot	1.4	26.98± 0.02	PS
	<i>z</i>	20111008	3	phot	1.4	25.78± 0.01	PS
J04402325-0530082	<i>i</i>	20120921	3	phot	0.8	27.01± 0.02	SDSS
	<i>z</i>	20120921	3	phot	0.9	25.83± 0.02	SDSS
J04433761+0002051	<i>i</i>	20121010	3	phot	0.8	26.85± 0.02	SDSS
	<i>z</i>	20121010	3	phot	0.9	25.70± 0.02	SDSS
J04440099-6624036	<i>i</i>	20110918	3	phot	0.9	26.87± 0.15	med
	<i>z</i>	20110918	3	phot	0.9	25.75± 0.15	med
J04480066-5041255	<i>i</i>	20121019	3	phot	1.4	26.87± 0.15	med
	<i>z</i>	20121019	3	phot	1.3	25.75± 0.15	med
J04533054-5551318	<i>i</i>	20120921	3	phot	1.1	26.87± 0.15	med
	<i>z</i>	20120921	3	phot	1.5	25.75± 0.15	med
J04571728-0621564	<i>i</i>	20111018	3	phot	1.0	26.87± 0.03	PS
	<i>z</i>	20111018	3	phot	0.9	25.73± 0.02	PS
J04593483+0147007	<i>i</i>	20121025	3	phot	1.4	26.83± 0.03	PS
	<i>z</i>	20121025	3	phot	1.4	25.75± 0.02	PS
J05090356-4209199	<i>i</i>	20120826,20121011	3	phot	1.3	26.82± 0.05	SM
	<i>z</i>	20120826,20121011	3	phot	1.2	25.69± 0.02	SM
J05100427-2340407	<i>i</i>	20121019	3	phot	1.4	26.88± 0.03	SM
	<i>z</i>	20121019	3	phot	1.3	25.79± 0.01	SM
J05142878-1514546	<i>i</i>	20111009	3	phot	0.8	26.90± 0.02	PS
	<i>z</i>	20111009	3	phot	0.7	25.81± 0.03	PS
J05241317-2104427	<i>i</i>	20111009	3	phot	0.7	26.93± 0.02	SM
	<i>z</i>	20111009	3	phot	0.6	25.78± 0.02	SM
J05241914-1601153	<i>i</i>	20121025	3	phot	1.3	26.82± 0.02	PS
	<i>z</i>	20121025	3	phot	1.3	25.75± 0.02	PS
J05254166-0909123	<i>i</i>	20121221	3	phot	0.9	26.83± 0.03	PS
	<i>z</i>	20121221	3	phot	0.9	25.72± 0.01	PS
J05332558-5117131	<i>i</i>	20110922	3	phot	1.1	26.87± 0.15	med
	<i>z</i>	20110922	3	phot	1.2	25.75± 0.15	med
J05335981-0221325	<i>i</i>	20121025	3	phot	1.2	26.80± 0.01	SDSS
	<i>z</i>	20121025	3	phot	1.3	25.71± 0.01	SDSS
J05392505-4245211	<i>i</i>	20111006	3	phot	0.9	26.87± 0.15	med
	<i>z</i>	20111006	3	phot	0.9	25.75± 0.15	med
J05395494-1307598	<i>i</i>	20121016	3	phot	0.9	26.89± 0.02	PS
	<i>z</i>	20121016	3	phot	0.9	25.83± 0.01	PS

Table 4 continued

Table 4 (*continued*)

Name	Filter	Obs. Date(s; UT) (YYYYMMDD)	N_{exp}	Condition ^a	FWHM "	Zero point	Source ^b
J05470650-3210413	<i>i</i>	20121012	3	phot	1.1	26.87± 0.15	med
	<i>z</i>	20121012	3	phot	1.0	25.75± 0.15	med
J05575096-1359503	<i>i</i>	20121010	3	phot	0.9	26.90± 0.02	PS
	<i>z</i>	20121010	3	phot	0.9	25.83± 0.02	PS
J06045215-3433360	<i>i</i>	20121023	4	phot	1.3	26.87± 0.15	med
	<i>z</i>	20121023	3	phot	1.1	25.75± 0.15	med
J06085283-2753583	<i>i</i>	20121012	3	phot	1.0	26.87± 0.02	SM
	<i>z</i>	20121012	3	phot	0.9	25.77± 0.01	SM
J06112997-7213388	<i>i</i>	20121221	3	phot	1.1	26.75± 0.02	SM
	<i>z</i>	20121221	3	phot	1.0	25.64± 0.02	SM
J06131330-2742054	<i>i</i>	20111009	3	phot	0.8	26.98± 0.02	SM
	<i>z</i>	20111009	3	phot	0.8	25.84± 0.01	SM
J06434532-6424396	<i>i</i>	20110923	3	phot	0.8	26.84± 0.04	SM
	<i>z</i>	20110923	3	phot	0.8	25.74± 0.02	SM
J08173943-8243298	<i>i</i>	20130103	3	phot	1.0	26.87± 0.15	med
	<i>z</i>	20130103	3	phot	1.0	25.75± 0.15	med
J08471906-5717547	<i>i</i>	20130103	3	phot	1.0	26.66± 0.01	SM
	<i>z</i>	20130103	3	phot	1.0	25.61± 0.01	SM
J10260210-4105537	<i>i</i>	20120203	3	phot	0.8	26.76± 0.02	SM
	<i>z</i>	20120203	3	phot	0.8	25.75± 0.01	SM
J10285555+0050275	<i>i</i>	20120204	3	phot	1.2	27.07± 0.03	SDSS
	<i>z</i>	20120204	3	phot	0.9	25.90± 0.03	SDSS
J11115267-4401538	<i>i</i>	20120203	3	phot	0.7	26.87± 0.15	med
	<i>z</i>	20120203	3	phot	0.8	25.75± 0.15	med
J11305355-4628251	<i>i</i>	20120205	3	phot	0.6	26.87± 0.15	med
	<i>z</i>	20120205	3	phot	0.6	25.75± 0.15	med
J11592786-4510192	<i>i</i>	20120204	3	phot	0.6	26.68± 0.03	SM
	<i>z</i>	20120204	3	phot	0.5	25.64± 0.02	SM
J12210499-7116493	<i>i</i>	20120205	3	phot	0.5	26.87± 0.15	med
	<i>z</i>	20120205	3	phot	0.5	25.75± 0.15	med
J12265135-3316124	<i>i</i>	20120204	3	phot	0.7	26.87± 0.15	med
	<i>z</i>	20120204	3	phot	0.7	25.75± 0.15	med
J12300521-4402359	<i>i</i>	20120204	3	phot	0.6	26.87± 0.15	med
	<i>z</i>	20120204	3	phot	0.6	25.75± 0.15	med
J12383713-2703348	<i>i</i>	20120204	3	phot	0.7	26.85± 0.02	SM
	<i>z</i>	20120204	3	phot	0.7	25.81± 0.01	SM
J14284804-7430205	<i>i</i>	20120205	3	phot	0.6	26.52± 0.04	SM
	<i>z</i>	20120205	3	phot	0.6	25.67± 0.01	SM
J14361471-7654534	<i>i</i>	20120205	3	phot	0.6	26.87± 0.15	med
	<i>z</i>	20120205	3	phot	0.5	25.75± 0.15	med
J15244849-4929473	<i>i</i>	20120229	3	phot	0.7	26.87± 0.15	med
	<i>z</i>	20120229	3	phot	0.7	25.75± 0.15	med
J15310958-3504571	<i>i</i>	20120229	3	phot	0.8	26.87± 0.15	med
	<i>z</i>	20120229	3	phot	0.8	25.75± 0.15	med
J16430128-1754274	<i>i</i>	20120304	3	lc	0.7	26.79± 0.01	PS
	<i>z</i>	20120304	3	phot	0.7	25.66± 0.01	PS
J16572029-5343316	<i>i</i>	20120305	3	phot	0.7	26.87± 0.15	med
	<i>z</i>	20120305	3	lc	0.7	25.75± 0.25	med

Table 4 continued

Table 4 (*continued*)

Name	Filter	Obs. Date(s; UT) (YYYYMMDD)	N_{exp}	Condition ^a	FWHM "	Zero point	Source ^b
J18420694-5554254	<i>i</i>	20120318	3	phot	1.3	26.74± 0.01	SM
	<i>z</i>	20120318	3	phot	1.3	25.63± 0.01	SM
J19225071-6310581	<i>i</i>	20120318	3	phot	1.3	26.69± 0.02	SM
	<i>z</i>	20120318	3	phot	1.2	25.64± 0.02	SM
J19355595-2846343	<i>i</i>	20120726	3	phot	1.0	26.81± 0.01	PS
	<i>z</i>	20120726	3	phot	1.0	25.71± 0.01	PS
J19560294-3207186	<i>i</i>	20120318	3	phot	1.0	26.87± 0.15	med
	<i>z</i>	20120318	3	phot	1.0	25.75± 0.15	med
J20004841-7523070	<i>i</i>	20120726	3	phot	1.4	26.87± 0.15	med
	<i>z</i>	20120726	3	phot	1.4	25.75± 0.15	med
J20013718-3313139	<i>i</i>	20110804	3	lc	0.7	26.87± 0.25	med
	<i>z</i>	20110804	3	phot	0.8	25.75± 0.15	med
J20100002-2801410	<i>i</i>	20110804	3	lc	0.8	26.84± 0.01	PS
	<i>z</i>	20110804	3	lc	0.7	25.59± 0.01	PS
J20333759-2556521	<i>i</i>	20110804	3	lc	0.9	26.78± 0.01	PS
	<i>z</i>	20110804	3	lc	0.8	25.55± 0.01	PS
J20465795-0259320	<i>i</i>	20110804	3	lc	1.1	26.90± 0.01	SDSS
	<i>z</i>	20110804	2	lc	0.9	25.70± 0.01	SDSS
J21100535-1919573	<i>i</i>	20110804	3	phot	0.9	26.97± 0.03	PS
	<i>z</i>	20110804	3	phot	0.9	25.84± 0.02	PS
J21265040-8140293	<i>i</i>	20120726,20120729	4	phot	1.4	26.87± 0.15	med
	<i>z</i>	20120726,20120729	3	phot	1.4	25.75± 0.15	med
J21471964-4803166	<i>i</i>	20110804	3	phot	1.3	26.89± 0.04	SM
	<i>z</i>	20110804	3	phot	1.1	25.81± 0.03	SM
J21521039+0537356	<i>i</i>	20120529	2	lc	1.0	26.56± 0.01	SDSS
	<i>z</i>	20120529	3	lc	0.9	25.57± 0.01	SDSS
J22021626-4210329	<i>i</i>	20110804	3	phot	1.0	26.87± 0.15	med
	<i>z</i>	20110804	3	phot	1.0	25.75± 0.15	med
J22440873-5413183	<i>i</i>	20120514	3	phot	1.1	26.71± 0.04	SM
	<i>z</i>	20120514	3	phot	1.6	25.71± 0.02	SM
J22470872-6920447	<i>i</i>	20120514	3	phot	0.9	26.87± 0.15	med
	<i>z</i>	20120514	3	phot	1.0	25.75± 0.15	med
J23131671-4933154	<i>i</i>	20120514	3	phot	1.4	26.87± 0.15	med
	<i>z</i>	20120514	3	phot	1.2	25.75± 0.15	med
J23221088-0301417	<i>i</i>	20120726	3	phot	1.2	26.79± 0.02	SDSS
	<i>z</i>	20120726	3	phot	1.2	25.63± 0.02	SDSS
J23285763-6802338	<i>i</i>	20120514	3	phot	1.1	26.87± 0.15	med
	<i>z</i>	20120514	3	phot	1.0	25.75± 0.15	med
J23301341-2023271	<i>i</i>	20120726	3	phot	1.6	26.78± 0.03	SDSS
	<i>z</i>	20120726	3	phot	1.0	25.52± 0.05	SDSS
J23320018-3917368	<i>i</i>	20120522	3	phot	1.2	26.88± 0.04	SM
	<i>z</i>	20120522	3	phot	0.9	25.71± 0.03	SM
J23452225-7126505	<i>i</i>	20120522	4	phot	1.0	26.87± 0.15	med
	<i>z</i>	20120522	4	lc	1.5	25.75± 0.25	med
J23474694-6517249	<i>i</i>	20120529	3	phot	1.0	26.87± 0.15	med
	<i>z</i>	20120529	3	phot	0.8	25.75± 0.15	med

Table 4 continued

Table 4 (*continued*)

Name	Filter	Obs. Date(s; UT) (YYYYMMDD)	N_{exp}	Condition ^a	FWHM "	Zero point	Source ^b
------	--------	--------------------------------	------------------	------------------------	-----------	------------	---------------------

^aThe observing condition was assigned based on the variation between the three or more exposures in the filter: photometric (phot) if the rms is $< 3\%$, or light clouds (lc) otherwise. See text for more details.

^bSource of the zero point fields calibrated with SDSS, SkyMapper, and Pan-STARRS are identified as SDSS, SM, and PS, respectively. Those without a direct calibration are identified as med, since the median of the zero points for all calibrated fields with photometric observations was assigned in those cases.

4. RESULTS

4.1. Candidate Companions

The flux-calibrated and median-combined i' and z' images were used to search for companions. All point sources were first identified on the z' images using the IDL procedure `find`. The position of each source was fine-tuned by fitting a 2D gaussian with `gcntrd`. The same sources were then identified in the i' images at the determined sky coordinates using the astrometries of the images. Sources identified in the z' image but not in the i' image are kept, since late-type candidates are not expected to be found in the i' image. The sky-subtracted flux in 1 FWHM apertures (the sky is sampled in an annulus between 2 and 3 FWHM) was determined for all sources in the i' and the z' images using aperture photometry. This flux was then converted to i' and z' magnitudes using the zero points determined previously (see Section 3.4). Sources that are too close to the edges of the images, with an extended PSF, or with saturated flux in i' or z' images, were excluded. The total number of sources retained varies substantially between the targets, between a few dozen to a few thousand. The $i' - z'$ of the sources was then computed. Only a lower limit for the $i' - z'$ color is available for sources not identified in the i' image.

At 5–10 Myr, the age of the youngest stars in the sample, the transition between planetary-mass and brown dwarfs takes place around the spectral types L1–L2. According to West et al. (2005), a typical L1–L2 dwarf has an $i' - z'$ color of about 1.8. Sources with $i' - z' > 1.7$ were thus conservatively selected. As seen in Section 3.4, there are targets for which the zero points of the i' and z' images are more uncertain. In the worst cases, the $i' - z'$ is expected to be off by 0.5 mag, considering the errors listed in Table 4. Two approaches were used in order to be sure to identify all plausible planetary-mass companions (with spectral type L0 and later) around these stars. In the first approach, the center of the $i' - z'$ distribution of all sources identified in the field was computed and artificially shifted to 0.5, which is the approximate $i' - z'$ of an early M, the typical star expected

in these far-red images Hawley et al. 2002; West et al. 2005. Then, all sources with (shifted) $i' - z'$ greater than 1.7 were inspected. In the second approach, the peak of the $i' - z'$ was left untouched, but all sources with $i' - z' > 1.2$ were inspected.

Considering the eccentricity distribution of Cumming et al. (2008) and random viewing time and inclination, it can be shown (see Section 4.3) that $< 2\%$ of candidates with projected distances > 8000 au will have a semimajor axis below 5000 au. Candidates with projected distances < 8000 au from the target were conservatively retained, to make sure all candidates with semimajor axis < 5000 au are identified. Most target stars are saturated in the GMOS z' image. To find their precise position, the R.A., decl. from the 2MASS catalog listed in Table 1 is used a first approximation. This position does not take into account the proper motion, so it is often off by several pixels (on average six to seven pixels but sometimes as much as several dozens of pixels). For stars that are unsaturated, a 2D Gaussian profile was fitted with IDL function `mpfit2dfun`; for the other stars, the position was found manually, fitting a circle region on the star.

These selection criteria were found to efficiently reject contaminants and left only a few candidates in any given field. Most of these were easily eliminated by a visual inspection of the median-combined and individual i' and z' images. Remaining false positives were likely cosmic rays or were located in the diffraction peaks of bright stars that affected their photometry. Some non-point-source objects that were not eliminated automatically with the criteria in the `find` procedure were also discarded. Other sources fall in part or entirely off the detectors in one or more of the individual images. Finally, the typical L and T colors and magnitudes shown in Figure 4 (West et al. 2005; Zhang et al. 2009) were helpful in discarding objects with $i' - z' > 1.7$ that are much too faint in z' to be brown dwarfs at the distance of the source. Only one candidate survived all selection criteria, around the M3 ABDMG star GU Psc (2MASS J01123504+1703557).

4.1.1. *GU Psc b*

GU Psc has an estimated age range of 130–200 Myr (given the most recent estimate of ABDMG age from [Bell et al. 2015](#)), and a corresponding statistical distance range of 45–49 pc. The characterization of the system is described by [Naud et al. \(2014\)](#) and only summarized here. GU Psc b was detected in the z' -band observations of 2011 September 22 ($z_{AB} = 21.76 \pm 0.07$), but not in the i' band. Follow-up observations with the same instrument and observational setup were made on 2011 October 18 to obtain a deeper i' -band image; four additional 300 s i' -band images were taken. The new i' -band imaging still did not reveal the companion but provided a 3σ upper limit on the flux of $i' > 25.28$, indicating a very red $i' - z'$ color (> 3.5 at 3σ). The $J_{Vega} = 18.15 \pm 0.05$ was measured at CFHT/WIRCam and the $K_s = 17.10 \pm 0.15$ was obtained with the 1.6 m Telescope of Observatoire du Mont-Mégantic. A spectrum was obtained with GNIRS at Gemini North, and a spectral type of T3.5 was assigned to the companion. The $J - K_s(\text{VEGA}) = 1.05 \pm 0.16$ is significantly redder than the bulk of field T dwarfs of comparable $z - J$, most likely because of the reduced collision-induced absorption by molecular hydrogen due to a low surface gravity. Using atmosphere models, the temperature and surface gravity were evaluated ($T_{\text{eff}}=1000\text{--}1100$ K and $\log g=4.18\text{--}4.36$). Using hot-start evolutionary models ([Saumon & Marley 2008](#); [Allard et al. 2013](#)), the mass was estimated to be in the range 9–13 M_{Jup} . Follow-up J -band observations allowed the confirmation of the common proper motion with the primary star, located $42''$ (2000 au) away from it.

4.2. *Detection limits*

The 5σ detection limits based on background brightness were evaluated for every median-combined z' -magnitude image as a function of angular separation. At each angular separation step, this value is the standard deviation of the sky-subtracted flux in 180 circular apertures (1 FWHM radii), at this distance, located all around the target. The flux in the sky was evaluated for each aperture using an annulus with a radius 2 and 3 times the FWHM. This yielded an upper limit on the flux that a companion could have without being detected at 5σ . The limiting magnitude is fainter at further separations from the star. A plateau is typically reached at an angular separation of $20''$ and lasts up to the limits of the field, at an angular separation of $\sim 155''$. The detection limits are shown in [Figure 5](#) and in [Table 5](#). Average distances, corresponding to the centers of the ranges given in [Table 2](#), were used to convert the angular separations to physical separations in astronomical units in the right panel of [Figure 5](#) and in [Table 5](#). For clarity of presentation, these central values were also used to convert the apparent magnitude to absolute magnitude in [Figure 5](#), while the full distance ranges were used to calculate the absolute magnitude ranges given in [Table 5](#). For the most distant stars, the plateau where the survey is the most sensitive is not reached before a projected distance of 1000 au or more and extends to separations that are well above 5000 au.

The masses corresponding to limiting magnitudes can then be computed from the age of each star using the substellar hot-start evolutionary models of [Baraffe et al. \(2003\)](#)⁴. The full ranges of absolute magnitudes, distances, and ages were used to assess the limiting mass ranges (see [Table 5](#)). The z' apparent magnitudes in the 21.5–23.9 range were reached on the plateau, with a median value of $z'=22.9$. Considering the average of the lower and upper values for the distance and age ranges listed in [Table 2](#), this corresponds to masses in the range 5–12 M_{Jup} .

Table 5. 5σ Detection limits

2MASS designation	Range of separation				Magnitude limit		Mass limit ^c (M_{Jup})
	min ($''$)	max ($''$)	min ^a (au)	max ^a (au)	Apparent z	Absolute z^b	
J00040288-6410358	4	150	208	7010	23.1	19.6–19.9	4.9– 5.5
J00172353-6645124	32	152	1284	5969	22.8	19.7–20.0	4.5– 4.9
J00325584-4405058	5	152	249	7040	23.0	19.1–20.6	3.6–11.7
J00374306-5846229	2	128	122	6371	22.8	18.9–19.9	3.1–12.2
J01071194-1935359	43	158	1786	6518	22.8	18.6–22.3	3.2–13.1

Table 5 continued

⁴ Available at <http://phoenix.ens-lyon.fr/Grids/BT-Settl/CIFIST2011/ISOCHRONES/>.

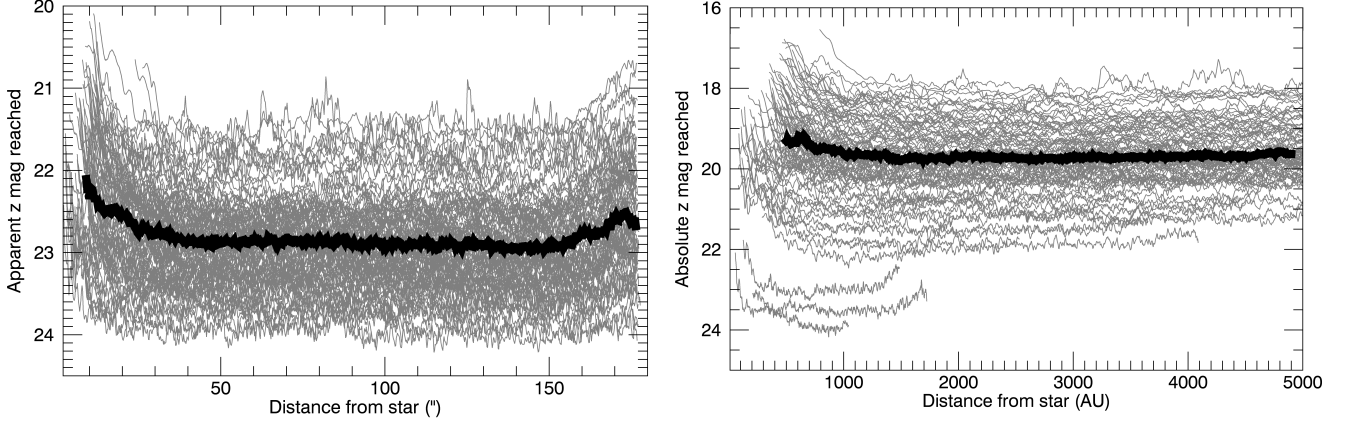


Figure 5. Left: apparent magnitude limit (5σ) as a function of angular separation for all stars in the sample. The median apparent magnitude on the plateau is $z'=22.9$. Right: corresponding absolute magnitudes and projected physical separations in au, computed with a distance equal to the mean of the ranges listed in Table 2. The median curves are plotted in black.

Table 5 (*continued*)

2MASS designation	Range of separation				Magnitude limit		Mass limit ^c (M_{Jup})
	min (")	max (")	min ^a (au)	max ^a (au)	Apparent z	Absolute z^b	
J01123504+1703557	20	155	950	7296	23.3	19.8–20.0	7.3– 9.4
J01132958-0738088	27	123	1360	6055	22.6	18.7–19.6	3.2–28.9
J01220441-3337036	32	144	1262	5647	21.8	18.7–18.9	6.0– 6.8
J01351393-0712517	26	164	999	6229	23.3	20.2–20.5	3.4– 4.5
J01415823-4633574	5	155	223	6265	22.9	19.7–20.0	4.8– 5.4
J01484087-4830519	30	166	1094	5993	22.8	19.9–20.1	7.1– 9.3
J01521830-5950168	27	153	1087	5977	22.7	19.6–19.8	5.0– 5.5
J02045317-5346162	10	104	424	4301	22.9	19.7–19.9	4.9– 5.4
J02070176-4406380	23	161	1020	6960	23.3	20.0–20.2	4.3– 4.9
J02155892-0929121	29	119	1252	5139	22.5	19.2–19.4	5.6– 6.0
J02215494-5412054	3	148	148	5794	23.4	20.2–20.6	3.7– 4.5
J02224418-6022476	26	156	816	4849	22.8	20.2–20.4	3.9– 4.6
J02251947-5837295	13	136	567	5803	22.0	18.7–19.0	6.0– 6.7
J02303239-4342232	36	157	1907	8196	23.3	19.6–19.8	5.1– 5.5
J02340093-6442068	3	148	151	6823	22.4	18.9–19.2	5.7– 6.3
J02485260-3404246	29	158	1271	6820	23.1	19.8–20.1	4.6– 5.3
J02564708-6343027	19	151	1074	8317	22.0	18.2–18.6	6.3– 8.0
J03050976-3725058	32	154	2348	11156	22.5	18.1–18.3	6.8– 8.1
J03350208+2342356	6	155	267	6597	23.1	19.9–20.1	4.4– 4.7
J03494535-6730350	21	154	1766	12524	23.3	18.7–18.9	6.0– 6.8
J04082685-7844471	19	98	1038	5335	22.7	19.0–19.0	5.8– 6.7
J04091413-4008019	24	140	1574	8842	22.6	18.4–18.7	6.1– 7.3
J04213904-7233562	28	160	1524	8525	22.6	18.8–19.2	5.8– 6.5
J04240094-5512223	36	158	2472	10619	23.2	18.9–19.2	5.7– 6.4
J04363294-7851021	15	121	885	6810	22.3	18.4–18.8	10.6–14.0
J04365738-1613065	33	150	760	3457	22.5	19.8–22.1	4.6– 5.3
J04402325-0530082	12	144	119	1412	23.4	23.5–23.5	< 3.2
J04433761+0002051	15	156	382	3988	23.1	20.8–21.4	2.2– 2.7
J04440099-6624036	14	177	797	9573	22.7	18.9–19.2	5.7– 6.4

Table 5 *continued*

Table 5 (*continued*)

2MASS designation	Range of separation				Magnitude limit		Mass limit ^c (M_{Jup})
	min (")	max (")	min ^a (au)	max ^a (au)	Apparent z	Absolute z^b	
J04480066-5041255	37	148	1975	7733	22.5	18.8–19.1	5.8– 6.6
J04533054-5551318	58	148	652	1650	22.4	22.1–22.2	2.5– 3.4
J04571728-0621564	22	107	1020	4848	22.8	19.4–19.7	8.0–10.7
J04593483+0147007	43	155	1121	4035	22.3	20.1–20.4	3.8– 4.5
J05090356-4209199	24	174	916	6450	22.8	19.1–21.4	2.3– 6.2
J05100427-2340407	42	155	2105	7612	22.5	18.9–19.3	5.5– 6.4
J05142878-1514546	10	172	657	10377	23.7	19.6–20.1	4.6– 5.5
J05241317-2104427	16	163	824	8326	23.7	20.0–20.4	3.9– 5.0
J05241914-1601153	37	168	705	3192	22.3	20.4–21.6	2.6– 4.0
J05254166-0909123	32	160	678	3323	23.1	21.3–21.8	3.2– 5.5
J05332558-5117131	33	141	1730	7378	22.9	19.1–19.5	5.5– 6.1
J05335981-0221325	29	144	1009	4924	22.3	19.4–19.9	4.5– 5.2
J05392505-4245211	25	161	1195	7498	23.2	19.5–20.4	3.9– 5.7
J05395494-1307598	11	160	804	10907	23.4	19.0–19.5	5.3– 6.2
J05470650-3210413	16	157	860	8209	22.9	19.1–19.7	5.2– 6.1
J05575096-1359503	21	153	864	6110	23.4	19.9–20.9	3.1–11.5
J06045215-3433360	31	146	265	1229	22.6	23.0–23.0	< 2.3
J06085283-2753583	5	160	159	4305	23.1	20.5–21.5	< 3.1
J06112997-7213388	12	153	606	7216	21.9	18.5–18.6	6.2– 7.7
J06131330-2742054	32	160	940	4726	23.5	21.1–21.3	2.2– 2.6
J06434532-6424396	24	176	1310	9546	23.5	19.6–20.0	4.7– 5.7
J08173943-8243298	39	156	1071	4232	22.9	20.6–20.9	2.3– 3.1
J08471906-5717547	16	166	368	3670	22.2	20.3–20.7	5.9– 8.3
J10260210-4105537	26	161	1645	9826	23.4	19.3–19.7	3.7– 4.4
J10285555+0050275	71	147	505	1041	23.2	23.9–23.9	< 2.3
J11115267-4401538	12	156	434	5333	23.4	20.3–21.2	3.7– 7.3
J11305355-4628251	7	160	435	9929	23.7	19.3–20.2	4.2– 9.1
J11592786-4510192	15	176	828	9723	23.9	19.8–20.7	3.1– 4.0
J12210499-7116493	23	157	2288	15464	23.6	18.4–18.9	3.3– 5.5
J12265135-3316124	15	175	1054	11594	23.6	19.4–19.6	3.7– 4.4
J12300521-4402359	11	177	809	12220	23.9	19.3–20.2	3.5– 4.4
J12383713-2703348	39	177	914	4087	23.6	21.7–21.9	2.9– 4.2
J14284804-7430205	19	171	909	7896	23.5	19.3–21.6	5.0–24.2
J14361471-7654534	17	173	629	6071	23.9	20.7–21.8	2.6–16.2
J15244849-4929473	13	175	320	4222	21.8	19.8–20.0	7.4– 9.6
J15310958-3504571	12	171	855	12031	23.2	18.6–19.5	3.4– 5.1
J16430128-1754274	12	161	516	6620	23.2	19.7–20.7	2.5–10.0
J16572029-5343316	12	176	670	9188	21.6	17.9–18.1	6.2– 7.1
J18420694-5554254	19	157	1007	8330	21.7	17.9–18.2	6.1– 7.0
J19225071-6310581	23	150	1329	8645	22.0	17.9–18.5	5.8– 9.0
J19355595-2846343	4	175	134	5445	22.7	19.8–20.8	3.1– 9.4
J19560294-3207186	42	159	2450	9250	22.5	18.5–18.8	5.4– 6.0
J20004841-7523070	12	150	399	4833	22.3	19.6–20.0	4.4– 5.0
J20013718-3313139	38	168	2375	10464	22.9	18.8–19.1	5.2– 5.7
J20100002-2801410	25	161	1236	7761	23.0	19.5–19.7	4.7– 5.1
J20333759-2556521	15	169	758	8182	22.9	19.4–19.7	4.7– 5.2
J20465795-0259320	26	161	1236	7430	23.0	19.6–19.8	7.8–10.1

Table 5 continued

Table 5 (*continued*)

2MASS designation	Range of separation				Magnitude limit		Mass limit ^c (M_{Jup})
	min (")	max (")	min ^a (au)	max ^a (au)	Apparent z	Absolute z ^b	
J21100535-1919573	45	170	1491	5629	23.5	20.7–21.0	2.1– 2.8
J21265040-8140293	3	148	103	4757	22.6	19.9–20.2	3.1– 9.4
J21471964-4803166	13	153	733	8453	22.9	18.7–19.9	4.6–12.8
J21521039+0537356	31	156	960	4768	22.7	19.9–20.7	5.9– 9.3
J22021626-4210329	35	164	1632	7554	23.0	19.6–19.9	5.0– 5.5
J22440873-5413183	20	137	979	6587	21.7	18.1–18.4	6.8– 8.0
J22470872-6920447	14	155	797	8531	22.5	18.7–18.9	10.2–13.0
J23131671-4933154	18	113	731	4556	22.6	19.5–19.7	5.3– 5.7
J23221088-0301417	35	155	1361	5891	22.8	19.5–20.4	3.6–23.0
J23285763-6802338	20	150	963	7211	22.8	19.2–19.5	5.5– 6.0
J23301341-2023271	46	154	760	2501	23.0	21.8–22.1	2.4– 2.5
J23320018-3917368	35	135	818	3127	23.3	21.4–21.6	3.6– 5.2
J23452225-7126505	14	154	652	6930	21.5	18.1–18.4	6.8– 8.2
J23474694-6517249	21	150	986	6904	23.1	19.7–19.9	5.0– 5.4

^aConsidering the average of the distance range given in Table 2

^bConsidering the full distance range given in Table 2

^cUsing the full distance and age ranges given in Table 2 in the Baraffe et al. (2003) evolutionary models.

For each target, it is possible to compute the fraction f_u of z' image pixels where a companion could have been detected at 5σ . This takes into account the bad pixels and background sources that hinder the detection of a companion. This quantity is represented in Figure 6 as a function of separation for all sample stars. It shows that beyond $10''$, typically more than 98% of putative companions should have been detected. For the stars that are the closest to the galactic plane, the density of objects is higher, and the fraction of objects that can be recovered can be lower (down to 96%). This is taken into account in the computation of completeness limits in Section 4.3.

4.3. Completeness Maps and Survey sensitivity

The detection limits in terms of absolute magnitudes and projected separations determined in Section 4.2 can be used to evaluate the sensitivity of the survey to planets of a given mass and semimajor axis. The method used here is similar to that described by Nielsen et al. (2008).

A Monte Carlo simulation was first used to build a completeness map for each star, that is, to assess what fraction of planets of a given mass and semimajor axis can be retrieved around it, considering the distribution of possible orbital parameters and considering its credible age and distance ranges. A grid of 100×100

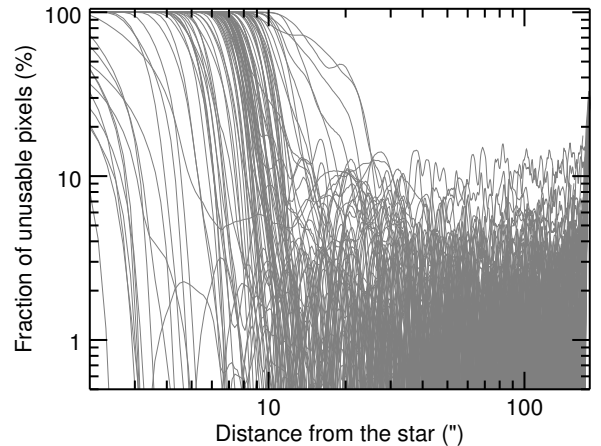


Figure 6. Fraction $1 - f_u$ of pixels where a companion cannot be found, considering bad pixels and background stars in the field. Beyond $\sim 10''$, $>98\%$ of putative companions would have been identified for the large majority of stars. A few low-galactic-latitude stars have a lower plateau value.

masses and semimajor axes was built, spread uniformly in log space, for masses between 3 and $100 M_{\text{Jup}}$ and semimajor axes of 100 to 5000 au. At each point of the grid, a population of 10,000 planets was simulated. The method described in Brandeker et al. (2006) and

Brandt et al. (2014) was used to determine the distribution of projected separations in astronomical units from the semimajor axes, given a distribution of eccentricity and assuming a random viewing angle and time of observation. The eccentricity distribution function adopted here is that of Cumming et al. (2008), that is, a uniform distribution between 0 and 0.8. The distance and age, sampled linearly within the ranges listed in Table 2, are used to convert physical projected separations to angular projected separations and to convert masses to absolute z' fluxes, using the evolutionary models of Baraffe et al. (2003). The 5σ detection curves computed in Section 4.2 (Figure 5) can then be used to determine whether or not a given simulated planet would be bright enough to be recovered around its host. If so, the fraction of pixels where a companion can be found f_u is taken as the detection probability. Repeating these steps for each simulated planet allows us to determine the fraction of planets that would have been detected around a star at each grid point. The resulting map is shown in Figure 7 for GU Psc.

Taking the sum of the maps for all stars allows us to assess the mean sensitivity for the entire survey (Figure 8), in terms of the fraction of stars in the survey for which a planet of a given mass and semimajor axis would have been detected. The figure demonstrates that the survey is most sensitive above 1000 au, with a peak between 2000 and 4000 au. The maximal detection probabilities are of 8%, 36%, 86%, 94%, and 95% for masses of 3, 5, 9, 11, and $13 M_{\text{Jup}}$, respectively. The survey is particularly sensitive to planets at the massive end of the planetary-mass range. The mean detection probabilities for $3 M_{\text{Jup}}$ companions are below 10% for all semimajor axes. At separations of ~ 500 au, the detection probabilities are nonnegligible: 10% for $5 M_{\text{Jup}}$ and 30% for $11 M_{\text{Jup}}$. The probability of finding a planet at 2000 au with the mass of GU Psc b ($\sim 11 M_{\text{Jup}}$) is over 90%. At 100–200 au, where most AO imaging surveys are most sensitive, the present survey has a small detection probability of less than 5%, even for the most massive planets.

4.4. Planet Frequency

Using the results presented in Section 4.3 and the statistical formalism presented in Lafrenière et al. (2007), it is possible to determine a credible interval for the fraction f of late spectral type (K5–L5) stars that have at least one companion in a given mass and semimajor axis range. If the $N = 95$ sample stars are enumerated by the set $\{d_j\}$, where the value of d is 1 for stars with a detected companion or 0 otherwise. The resulting set $\{d_j\}$ depends on the true fraction of stars f that host a planet in the surveyed range of semimajor axes and

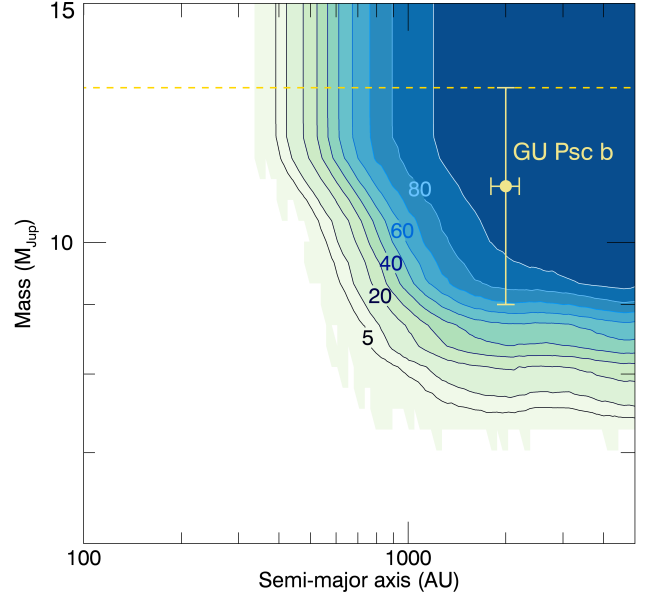


Figure 7. Completeness map for the star GU Psc. The contours indicate the fraction of planets that would be recovered in percent, considering a uniform eccentricity distribution between 0 and 0.8, a random inclination and time of observation, the distance and age ranges given in Table 2, and the hot-start models of Baraffe et al. (2003). The horizontal dashed line is the $13 M_{\text{Jup}}$ separation between planetary-mass objects and brown dwarfs.

masses. It is given by the binomial likelihood:

$$\mathcal{L}(\{d_j\}|f) = \prod_{j=1}^N (1 - fp_j)^{(1-d_j)} (fp_j)^{d_j} \quad (1)$$

The completeness maps (as shown for GU Psc b in Figure 7) are used to determine p_j , which represents the probability of detecting a companion with a mass in a given range $[m_{\text{min}}, m_{\text{max}}]$ and a semimajor axis in a given range $[a_{\text{min}}, a_{\text{max}}]$. For each star, p_j is taken to be the mean of the recovered planet fraction in all grid points for the mass and semimajor axis ranges considered. Since the grid is uniform in log mass and log a , this is equivalent to assuming log-uniform distributions for these two parameters. Bayes' theorem states that the posterior distribution, which is the probability density function of f considering the results of the survey $\{d_j\}$, is given by

$$P(f|\{d_j\}) = \frac{\mathcal{L}(\{d_j\}|f)P(f)}{\int_0^1 \mathcal{L}(\{d_j\}|f)P(f)df}. \quad (2)$$

The denominator can be referred to as the *marginalized likelihood*. The prior distribution $P(f)$ represents the best knowledge on the probability density for f using only information independent from the current survey. In several direct imaging survey analyses, a flat prior

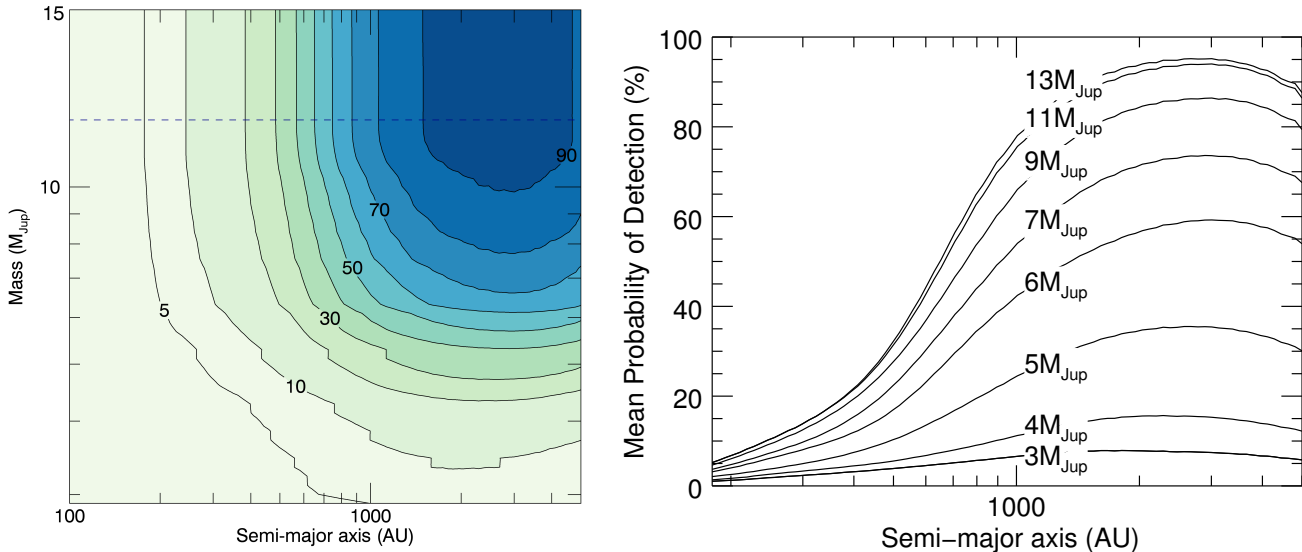


Figure 8. Completeness map and mean detection probability for the survey. The left panel gives the mean detection probability in percentage with respect to mass and semimajor axis. The horizontal dashed line is the $13 M_{\text{Jup}}$ separation between planetary-mass objects and brown dwarfs. The right panel shows the mean probability of detection vs. semimajor axis, for specific values of companion mass.

distribution $P(f) = 1$ was used. While simpler, a uniform prior is in general not mathematically equivalent to having no prior knowledge on the parameters. As an illustration of this concept, a change of coordinates can result in a different answer if a flat prior is used in both coordinate systems, and therefore the resulting posterior does not only depend on the likelihood model and the available data, but also depends on the way that the problem is parameterized. Applying Bayesian statistics in a way that only depends on the available data and the likelihood model requires using non-informative priors (e.g., see Berger et al. 2009), which do not always correspond to flat priors. In a case with only one parameter, the non-informative prior can be derived in a simple way and is called Jeffrey’s prior (see Jeffreys 1998). The Jeffrey’s prior that is associated with the binomial likelihood is given by

$$P(f) = \frac{1}{\pi} \frac{1}{\sqrt{f}} \frac{1}{\sqrt{1-f}}. \quad (3)$$

As shown in Figure 8, the survey is particularly sensitive for semimajor axes between 500 and 5000 au and masses between 5 and $13 M_{\text{Jup}}$. The posterior distribution was thus computed for these ranges and is shown in Figure 9. This accounts for the detection of a single companion (GU Psc b) in these intervals. Only the projected separation of the companion (2000 au) is known, but considering the eccentricity distribution of Cumming et al. (2008) and the random viewing time and inclination as in Section 4.3, it can be shown that the

semimajor axis of the companion is unlikely to have a semimajor axis above 5000 au. The peak of this posterior distribution corresponds to the most likely value of f . Given a level of confidence α , an equal-tail credible interval $[f_{\min}, f_{\max}]$ can be determined using

$$\frac{1 - \alpha}{2} = \int_0^{f_{\min}} p(f|\{d_j\})df, \quad (4)$$

$$\frac{1 + \alpha}{2} = \int_{f_{\max}}^1 p(f|\{d_j\})df. \quad (5)$$

The fraction of late spectral type (K5–L5) stars that have at least one companion in this semimajor axis and mass ranges is $0.84^{+6.73\%}_{-0.66\%}$ ($\alpha=95\%$). Note that if a flat prior had been assumed, the planet frequency would have been artificially larger with a wider confidence interval ($1.66^{+7.22\%}_{-1.27\%}$).

5. DISCUSSION

The sensitivity of the present survey to planetary-mass companions ($5\text{--}13 M_{\text{Jup}}$) is maximized between 500 and 5000 au, much farther than typical AO-assisted imaging surveys around similar stars, which are sensitive to up to 1000 au at best. The small overlap can be used to compare the limits on the occurrence of companions around young M stars, and to study this occurrence as a function of the separation from the central star.

The meta-analysis of Bowler (2016) puts an upper limit of $< 7.3\%$ (95% confidence level) on the frequency of $5\text{--}13 M_{\text{Jup}}$ companions at separations between 100 and 1000 au around M stars. An analysis similar to that

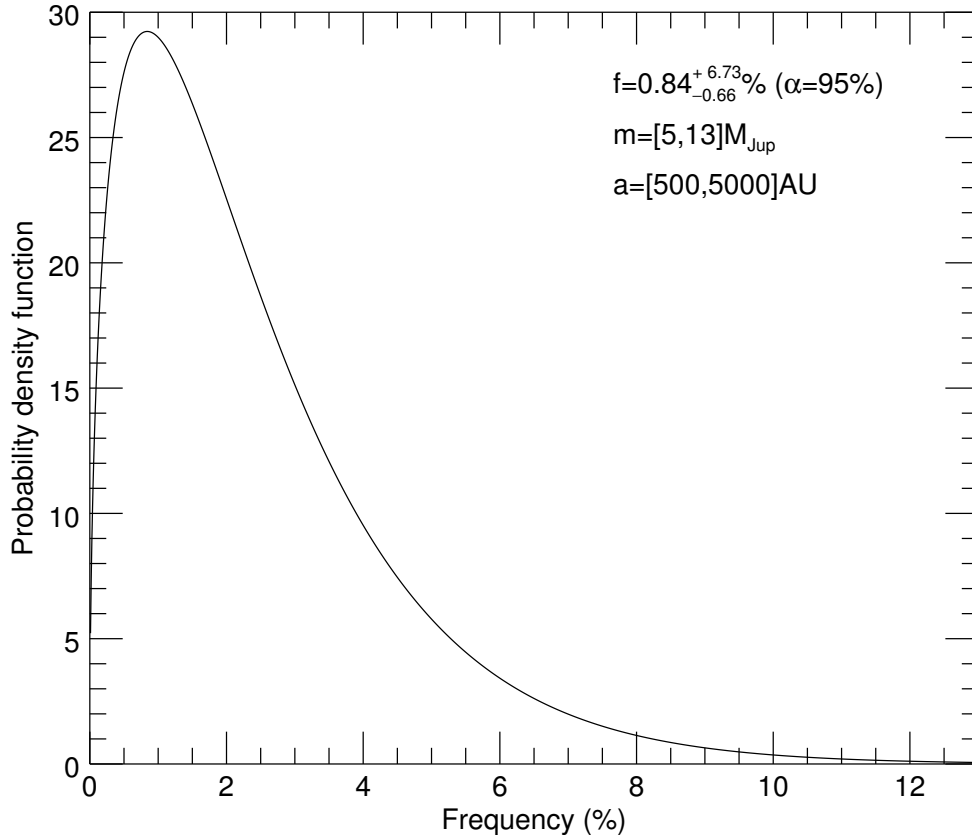


Figure 9. Probability density function for the frequency of late spectral type (K5–L5) stars with at least a companion with masses in the range $m = [5, 13] M_{\text{Jup}}$ and semimajor axes in the range $a = [500, 5000]$ au.

presented in Section 4.4 and based on the present survey data was carried for these ranges. Only an upper limit was determined because GU Psc b is in all likelihood outside this range of semimajor axes considering the method described in Section 4.3 (there is less than a 15% chance that GU Psc b has a semimajor axis below 1000 au with a projected separation of 2000 au). An upper limit of $< 11.1\%$ was found at the same confidence level. This is consistent with the Bowler (2016) result. The Bowler (2016) survey is more constraining because it includes more stars (119 compared to 95), but also because the present survey is only moderately sensitive in these ranges: the average detection probability for $13 M_{\text{Jup}}$ at 1000 au is close to 80% but only 25% for $5 M_{\text{Jup}}$. Lafrenière et al. (2007) derived an analytical expression for the planet frequency f_{max} in the special case of nondetections:

$$f_{\text{max}} \sim \frac{-\ln(1-\alpha)}{N\langle p_j \rangle}, \quad (6)$$

where $\langle p_j \rangle$ is the average planet detection probability, N the total number of stars in the survey, and α the confidence interval level. This approximation is valid for $N\langle p_j \rangle \gg 1$. Since the same intervals were used in the present survey and the Bowler (2016) analysis, both results can be combined, assuming $\alpha = 0.95$, to derive an upper limit of $< 4.4\%$ for the fraction of late spectral type (K5–L5) stars with at least a giant planetary-mass companion in the mass range $[5, 13] M_{\text{Jup}}$ with semimajor axis < 1000 au.

Lannier et al. (2016) found that $2.3^{+2.9}_{-0.7}\%$ (1σ confidence) of M stars have a $2\text{--}14 M_{\text{Jup}}$ companion between 8 and 400 au. The present survey is not sensitive to companions between 2 and $5 M_{\text{Jup}}$ and below 400 au, so it is not relevant to compute a frequency in this range of parameters. It is, however, interesting to note that the fraction obtained by Lannier et al. (2016) is similar to that found here for more massive and more distant planets. It is also similar to the $2^{+3}_{-1}\%$ frequency

derived from radial velocity data (Bonfils et al. 2011) for less massive giant planets (up to $\sim 3 M_{\text{Jup}}$) very close to low-mass older stars (periods between 10 and 100 days; main-sequence stars). All planet surveys so far have demonstrated that gas giants are rare beyond ~ 10 au around low-mass stars, as expected from planet formation models. The survey presented here yielded a planet frequency similar to those found for closer-in planets within uncertainties, although it spans a much wider separation interval. The planet frequency thus seems to remain similar over three orders of magnitude in orbital separations, despite the fact that planets in these regimes likely form through different mechanisms.

There is no agreement at this stage as to whether planetary-mass companions at wide separations are correlated with the stellar mass, as suggested for closer-in companions (Johnson et al. 2007; Borucki et al. 2011). Lannier et al. (2016) find that such a correlation probably exists for substellar companions that have a low mass ratio ($Q < 1\%$). This is in agreement with the conclusion of Montet et al. (2014; from a combination of direct imaging and radial velocity) and Clanton & Gaudi (2014; combination of microlensing and radial velocity), that giant planets are less frequent around low-mass stars. However, they do not find evidence for a correlation at higher mass ratio values ($1\% < Q < 5\%$). GU Psc b, with $Q \sim 3\%$, falls in that regime. In their meta-analysis, Bowler (2016) and Galicher et al. (2016) do not find evidence that there are fewer giant planets around low-mass stars; in both surveys, the frequencies derived for host stars of different masses are compatible with each other. While the present survey confirms the existence – albeit rare – of planetary-mass companions at wide separations, more detections are required to determine whether the presence of these are correlated with stellar host mass.

6. CONCLUSION

The PSYM-WIDE survey allowed us to search for planetary-mass companions around 95 low-mass stars (spectral types K5–L5) that are members of young associations. It used Gemini GMOS i' and z' imaging to identify them via their distinctively red $i' - z'$ color and allowed us to establish a frequency of stars with at least one companion of $0.84^{+6.73\%}_{-0.66\%}$ (95% confidence) in the mass range 5–13 M_{Jup} and with semimajor axes range 500–5000 au.

The only planet discovered through this survey (GU Psc b; Naud et al. 2014) and other substellar companions discovered via direct imaging (e.g., the $\sim 23 M_{\text{Jup}}$ brown dwarf HIP 78530 B; Lafrenière et al. 2008, 2010 or Ross 458 (AB) c, a distant planetary-mass companion to a M0.5+M7 binary, (Burgasser et al. 2010; Goldman et al. 2010) are too widely separated from their

stars for in situ formation by either core accretion or gravitational instability. This suggests that other mechanisms, such as direct formation through the turbulent fragmentation of a prestellar core (Padoan & Nordlund 2002; Bate et al. 2003) or ejection through interaction with a massive companion, could be at play in these cases.

As demonstrated by the in-depth photometric and spectroscopic study of GU Psc b (Naud et al. 2014) and the study of its light curve evolution Naud et al. (2017), wide planetary-mass companions are amenable to a level of characterization that is useful in assessing the characteristics of closer-in giant planets, which are much harder to study. Further surveys to identify wide-separation exoplanets would be valuable, especially deeper ones that are focused on the identification of less-massive giant planets. New detections would contribute to investigating possible correlations with the mass of the host star, and more generally the various formation mechanisms at play. The WEIRD survey (Wide orbit Exoplanet search with InfraRed Direct imaging; Baron et al. 2015), an ongoing effort using Spitzer and ground-based facilities such as CFHT and Gemini, will provide better constraints on the presence of these very wide (>500–1000 au) planetary-mass companions. The observations are obtained at 3.6 and 4.5 μm and are thus sensitive to planets down to about the mass of Saturn ($0.3 M_{\text{Jup}}$).

ACKNOWLEDGMENTS

The authors would like to thank Julien Rameau for his valuable suggestions and helpful discussions. They are also very grateful for the help of the Pan-STARRS1 and SkyMapper teams for providing data and the support for using it to do the photometric calibration of the data. They would also like to thank the anonymous referee for constructive comments and suggestions that improved the overall quality of the paper. This work was financially supported by the Natural Sciences and Engineering Research Council (NSERC) of Canada and the Fond de Recherche Québécois - Nature et Technologie (FRQNT; Québec). This publication makes use of data products from the Two Micron All Sky Survey, which is a joint project of the University of Massachusetts and the Infrared Processing and Analysis Center, and funded by the National Aeronautics and Space Administration and the National Science Foundation, of the NASA Astrophysics Data System Bibliographic Services, the VizieR catalog access tool, and the SIMBAD database operated at CDS, Strasbourg, France. It also made use of the L and T dwarf data archive <http://staff.gemini.edu/~sleggett/LTdata.html>.

This work also used data from the Sloan Digital Sky Survey III (SDSS-III). Funding for this survey has been

provided by the Alfred P. Sloan Foundation, the Participating Institutions, the National Science Foundation, and the U.S. Department of Energy Office of Science. The SDSS-III web site is <http://www.sdss3.org/>. SDSS-III is managed by the Astrophysical Research Consortium for the Participating Institutions of the SDSS-III Collaboration including the University of Arizona, the Brazilian Participation Group, Brookhaven National Laboratory, University of Cambridge, University of Florida, the French Participation Group, the German Participation Group, the Instituto de Astrofísica de Canarias, the Michigan State/Notre Dame/JINA Participation Group, Johns Hopkins University, Lawrence Berkeley National Laboratory, Max Planck Institute for Astrophysics, New Mexico State University, New York University, Ohio State University, Pennsylvania State University, University of Portsmouth, Princeton University, the Spanish Participation Group, University of Tokyo, University of Utah, Vanderbilt University, University of Virginia, University of Washington, and Yale University.

Data products from the Pan-STARRS were also used. PS1 has been made possible through contributions of the Institute for Astronomy, the University of Hawaii, the Pan-STARRS Project Office, the Max Planck Society and its participating institutes, the Max Planck Institute for Astronomy, Heidelberg, and the Max Planck Institute for Extraterrestrial Physics, Garching, The Johns Hopkins University, Durham University, the Uni-

versity of Edinburgh, Queen's University Belfast, the Harvard-Smithsonian Center for Astrophysics, the Las Cumbres Observatory Global Telescope Network Incorporated, the National Central University of Taiwan, the Space Telescope Science Institute, the National Aeronautics and Space Administration under Grant No. NNX08AR22G issued through the Planetary Science Division of the NASA Science Mission Directorate, the National Science Foundation under Grant No. AST-1238877, the University of Maryland, and Eotvos Lorand University (ELTE), and the Los Alamos National Laboratory.

Finally, SkyMapper data products were used. The national facility capability for SkyMapper has been funded through ARC LIEF grant LE130100104 from the Australian Research Council, awarded to the University of Sydney, the Australian National University, Swinburne University of Technology, the University of Queensland, the University of Western Australia, the University of Melbourne, Curtin University of Technology, Monash University, and the Australian Astronomical Observatory. SkyMapper is owned and operated by The Australian National University's Research School of Astronomy and Astrophysics. The survey data were processed and provided by the SkyMapper Team at ANU. The SkyMapper node of the All-Sky Virtual Observatory is hosted at the National Computational Infrastructure (NCI).

REFERENCES

- Ahn, C. P., Alexandroff, R., Allende Prieto, C., et al. 2012, *ApJS*, 203, 21
- Albert, L., Artigau, É., Delorme, P., et al. 2011, *ApJ*, 141, 203
- Allard, F., Homeier, D., Freytag, B., Schaffenberger, & Rajpurohit, A. S. 2013, *MSAIS*, 24, 128
- Allen, P. R., Koerner, D. W., Reid, I. N., & Trilling, D. E. 2005, *ApJ*, 625, 385
- Allers, K. N., & Liu, M. C. 2013, *ApJ*, 772, 79
- Anderson, E., & Francis, C. 2012, *AstL*, 38, 331
- Artigau, É., Lafrenière, D., Doyon, R., et al. 2007, *AJ*, 659, L49
- Bailey, J. I., White, R. J., Blake, C. H., et al. 2012, *ApJ*, 749, 16
- Baraffe, I., Chabrier, G., Barman, T. S., Allard, F., & Hauschildt, P. H. 2003, *A&A*, 402, 701
- Baron, F., Artigau, É., Rameau, J., et al. 2015, *American Astronomical Society*, 3, 104.09
- Bate, M. R., Bonnell, I. A., & Bromm, V. 2003, *MNRAS*, 339, 577
- Bell, C. P. M., Mamajek, E. E., & Naylor, T. 2015, *MNRAS*, 454, 593
- Berger, J. O., Bernardo, J. M., & Sun, D. 2009, *The Annals of Statistics*
- Bergfors, C., Brandner, W., Janson, M., et al. 2010, *AJ*, 520, A54
- Beuzit, J.-L., Feldt, M., Dohlen, K., et al. 2008, in *Proc. SPIE*, ed. I. S. Mclean & M. M. Casali (SPIE), 701418–701418–12
- Biller, B. A., Liu, M. C., Wahhaj, Z., et al. 2013, *ApJ*, 777, 160
- Bonfils, X., Delfosse, X., Udry, S., et al. 2011, *A&A*, 549, 5019
- Borucki, W. J., Koch, D. G., Basri, G. S., et al. 2011, *ApJ*, 736, 19
- Bowler, B. P. 2016, *PASP*, 128, 102001
- Bowler, B. P., Liu, M. C., Shkolnik, E. L., & Tamura, M. 2015, *ApJS*, 216, 7
- Brandeker, A., Jayawardhana, R., Khavari, P., Haisch Jr, K. E., & Mardones, D. 2006, *ApJ*, 652, 1572
- Brandt, T. D., Kuzuhara, M., McElwain, M. W., et al. 2014, *ApJ*, 786, 1
- Burgasser, A. J., Simcoe, R. A., Bochanski, J. J., et al. 2010, *ApJ*, 725, 1405
- Caballero, J. A., Béjar, V. J. S., Rebolo, R., et al. 2007, *ApJ*, 470, 903
- Chabrier, G., Baraffe, I., Allard, F., & Hauschildt, P. 2000, *ApJ*, 542, 464
- Chauvin, G., Lagrange, A. M., Dumas, C., et al. 2004, *A&A*, 425, L29
- Chauvin, G., Lagrange, A. M., Bonavita, M., et al. 2010, *AJ*, 509, A52
- Chauvin, G., Vigan, A., Bonnefoy, M., et al. 2015, *A&A*, 573, A127
- Clanton, C., & Gaudi, B. S. 2014, *ApJ*, 791, 91
- Cruz, K. L., Kirkpatrick, J. D., & Burgasser, A. J. 2009, *AJ*, 137, 3345
- Cruz, K. L., Reid, I. N., Liebert, J., Kirkpatrick, J. D., & Lowrance, P. J. 2003, *AJ*, 126, 2421

- Cruz, K. L., Reid, I. N., Kirkpatrick, J. D., et al. 2007, *AJ*, 133, 439
- Cumming, A., Butler, R. P., Marcy, G. W., et al. 2008, *PASP*, 120, 531
- Cutri, R. M., Skrutskie, M. F., van Dyk, S., et al. 2003, *VizieR Online Data Catalog*, 2246, 0
- Delorme, P., Lagrange, A. M., Chauvin, G., et al. 2012, *A&A*, 539, A72
- Delorme, P., Willott, C. J., Forveille, T., et al. 2008, *A&A*, 484, 469
- Dhital, S., West, A. A., Stassun, K. G., & Bochanski, J. J. 2010, *AJ*, 139, 2566
- Donaldson, J. K., Weinberger, A. J., Gagné, J., et al. 2016, eprint arXiv:1610.01667, 1610.01667
- Ducourant, C., Teixeira, R., Chauvin, G., et al. 2008, *A&A*, 477, L1
- Epchtein, N., de Batz, B., Capoani, L., et al. 1997, *The Messenger*, 87, 27
- Faherty, J. K., Burgasser, A. J., Walter, F. M., et al. 2012, *AJ*, 752, 56
- Faherty, J. K., Riedel, A. R., Cruz, K. L., et al. 2016, eprint arXiv:160507927, 160507927
- Gagné, J., Burgasser, A. J., Faherty, J. K., et al. 2015a, *ApJL*, 808, L20
- Gagné, J., Lafrenière, D., Doyon, R., Malo, L., & Artigau, É. 2014, *ApJ*, 783, 121
- . 2015b, *ApJ*, 798, 73
- Gagné, J., Faherty, J. K., Cruz, K. L., et al. 2015c, *ApJS*, 219, 33
- Galicher, R., Marois, C., Macintosh, B., et al. 2016, arxiv.org, arXiv:1607.08239
- Gizis, J. E. 2002, *ApJ*, 575, 484
- Goldman, B., Marsat, S., Henning, T., Clemens, C., & Greiner, J. 2010, *MNRAS*, 405, 1140
- Gontcharov, G. A. 2006, *AstL*, 32, 759
- Hawley, S. L., Covey, K. R., Knapp, G. R., et al. 2002, *AJ*, 123, 3409
- Hook, I. M., Jørgensen, I., Allington Smith, J. R., et al. 2004, *PASP*, 116, 425
- Janson, M., Horrmuth, F., Bergfors, C., et al. 2012, *ApJ*, 754, 44
- Jeffreys, H. 1998, *The Theory of Probability* (OUP Oxford)
- Johnson, J. A., Butler, R. P., Marcy, G. W., et al. 2007, *ApJ*, 670, 833
- Kirkpatrick, J. D., Looper, D. L., Burgasser, A. J., et al. 2010, *ApJS*, 190, 100
- Kiss, L. L., Moór, A., Szalai, T., et al. 2011, *MNRAS*, 411, 117
- Koen, C., Kilkeny, D., van Wyk, F., & Marang, F. 2010, *MNRAS*, 403, 1949
- Lafrenière, D., Jayawardhana, R., & van Kerkwijk, M. H. 2008, *ApJL*, 689, L153
- . 2010, *ApJ*, 719, 497
- Lafrenière, D., Doyon, R., Marois, C., et al. 2007, *ApJ*, 670, 1367
- Lannier, J., Delorme, P., Lagrange, A. M., et al. 2016, *A&A*
- Macintosh, B., Graham, J. R., Ingraham, P., et al. 2014, in *Proceedings of the National Academy of Sciences, Lawrence Livermore National Laboratory, Livermore, CA 94551*; Kavli Institute for Particle Astrophysics and Cosmology, Stanford University, Stanford, CA 94305, 12661–12666
- Macintosh, B., Graham, J. R., Barman, T. S., et al. 2015, *Science*, 350, 64
- Magnier, E. A., Schlafly, E., Finkbeiner, D., et al. 2013, *ApJS*, 205, 20
- Makarov, V. V., & Urban, S. 2000, *MNRAS*, 317, 289
- Malo, L., Artigau, É., Doyon, R., et al. 2014a, *ApJ*, 788, 81
- Malo, L., Doyon, R., Feiden, G. A., et al. 2014b, *ApJ*, 792, 37
- Malo, L., Doyon, R., Lafrenière, D., et al. 2013, *ApJ*, 762, 88
- Marois, C., Macintosh, B., Barman, T. S., et al. 2008, *Science*, 322, 1348
- Marois, C., Zuckerman, B., Konopacky, Q. M., Macintosh, B., & Barman, T. S. 2010, *Nature*, 468, 1080
- Mayor, M., & Queloz, D. 1995, *Nature*, 378, 355
- Montet, B. T., Crepp, J. R., Johnson, J. A., Howard, A. W., & Marcy, G. W. 2014, *ApJ*, 781, 28
- Naud, M.-E., Artigau, É., Rowe, J. F., et al. 2017, *AJ*, 154, 138
- Naud, M.-E., Artigau, É., Malo, L., et al. 2014, *ApJ*, 787, 5
- Nielsen, E. L., Close, L., Biller, B. A., Masciadri, E., & Lenzen, R. 2008, *ApJ*, 674, 1
- Padoan, P., & Nordlund, Å. 2002, *ApJ*, 576, 870
- Radigan, J., Lafrenière, D., Jayawardhana, R., & Doyon, R. 2009, *ApJ*, 698, 405
- Reid, I. N., Cruz, K. L., Burgasser, A. J., & C Liu, M. 2008, *AJ*, 135, 580
- Reid, I. N., Kirkpatrick, J. D., Liebert, J., et al. 2002, *AJ*, 124, 519
- Reylé, C., Delorme, P., Willott, C. J., et al. 2010, *A&A*, 522, A112
- Riaz, B., Gizis, J. E., & Harvin, J. 2006, *AJ*, 132, 866
- Rice, E. L., Faherty, J. K., & Cruz, K. L. 2010, *AJ*, 715, L165
- Riedel, A. R., Murphy, S. J., Henry, T. J., et al. 2011, *AJ*, 142, 104
- Riedel, A. R., Finch, C. T., Henry, T. J., et al. 2014, *AJ*, 147, 85
- Rodriguez, D. R., Bessell, M. S., Zuckerman, B., & Kastner, J. H. 2011, *ApJ*, 727, 62
- Roeser, S., Demleitner, M., & Schilbach, E. 2010, *AJ*, 139, 2440
- Saumon, D., & Marley, M. S. 2008, *ApJ*, 689, 1327
- Schlafly, E. F., Finkbeiner, D. P., Jurić, M., et al. 2012, *ApJ*, 756, 158
- Schmidt, S. J., Cruz, K. L., Bongiorno, B. J., Liebert, J., & Reid, I. N. 2007, *AJ*, 133, 2258
- Shkolnik, E. L., Anglada-Escude, G., Liu, M. C., et al. 2012, *AJ*, 758, 56
- Shkolnik, E. L., Liu, M. C., Reid, I. N., Dupuy, T. J., & Weinberger, A. J. 2011, *ApJ*, 727, 6
- Tonry, J. L., Stubbs, C. W., Lykke, K. R., et al. 2012, *ApJ*, 750, 99
- Torres, C. A. O., Quast, G. R., da Silva, L., et al. 2006, *A&A*, 460, 695
- van Leeuwen, F. 2007, *A&A*, 474, 653
- Wagner, K., Apai, D., Kasper, M., et al. 2016, *Science*, 353, aaf9671
- Weis, E. W. 1991, *AJ*, 102, 1795
- West, A. A., Hawley, S. L., Bochanski, J. J., et al. 2008, *AJ*, 135, 785
- West, A. A., Walkowicz, L. M., & Hawley, S. L. 2005, *PASP*, 117, 706
- Wolf, C., Onken, C. A., Schmidt, B. P., et al. 2016, *SkyMapper Early Data Release*
- Zacharias, N., Finch, C. T., Girard, T. M., et al. 2012, *VizieR On-line Data Catalog*, 1322
- Zacharias, N., Monet, D. G., Levine, S. E., et al. 2005, *VizieR Online Data Catalog*, 1297, 0
- Zhang, Z. H., Pokorny, R. S., Jones, H. R. A., et al. 2009, *A&A*, 497, 619
- Zuckerman, B., & Song, I. 2004, *ARA&A*, 42, 685